Table 1 Description of the patients

Case number	Age at death (year)	Age at onset (year)	Sex	Family history	Brain weight (g)	Clinical diagnosis	Region
ALS							
1	62	61	M	N	1150	ALS	Prec, L and other regions[a]
2	72	71	F	N	1390	ALS	Prec and L
3	42	40	F	N	1140	ALS	Prec, L and other regions[a]
4	76	75	F	N	NA	ALS	Prec and L
5	62	54	M	N	1230	ALS	Prec and other regions[a]
6	77	76	F	N	NA	ALS	Prec
7	67	65	M	N	1414	ALS	Fr
8	55	53	M	Y(m*C9ORF72*)	1250	ALS	Fr
FTLD-TDP type A							
9	58	49	M	Y(m*C9ORF72*)	1050	FTD	Fr
10	67	54	F	Y(m*GRN*)	NA	FTD	Fr
11	71	63	F	Y(m*GRN*)	863	PNFA	Fr
12	66	56	F	Y(m*GRN*)	1100	FTD	Fr
13	68	60	M	Y(m*GRN*)	1210	FTD + MND	Fr
FTLD-TDP type B							
14	45	43	M	N	1260	FTD + MND	Fr
15	59	57	M	Y(m*C9ORF72*)	1210	FTD + MND	Fr
16	67	65	M	N	1280	FTD + MND	Fr
17	76	74	M	N	1215	FTD + MND	Fr
18	69	58	M	N	1166	FTD + MND	Fr
19	52	50	F	Y(m*C9ORF72*)	1050	FTD + MND	Fr
20	65	61	M	N	1530	FTD + MND	Fr
21	68	64	M	N	1213	FTD + MND	Fr
FTLD-TDP type C							
22	82	NA	M	N	1200	SD	Fr, Te and other regions[b]
23	67	65	M	N	NA	SD	Fr
24	59	53	M	N	NA	SD	Fr
25	63	58	M	N	NA	SD	Fr
26	66	55	F	N	1035	SD	Fr
27	75	60	M	N	1174	SD	Fr
AD							
28	65	56	F	N	1165	AD	Fr
29	70	NA	F	N	1126	AD	Fr

AD = Alzheimer's disease; Fr = frontal cortex; FTD = frontotemporal dementia; L = lumbar part of spinal cord; m*C9ORF72* = mutation of chromosome 9 open-reading frame 72 gene; m*GRN* = mutation of progranulin gene; MND = motor neuron disease; NA = not available; PNFA = progressive non-fluent aphasia; Prec = precentral gyrus; SD = semantic dementia; Y = yes; N = no.

a Other regions contained striatum, thalamus, hippocampus dentate gyrus, substantia nigra, pons, medulla and cerebellum cortex. In these cases, the grey and white matter of precentral gyrus were separated from each other macroscopically and examined.

b Other regions contain striatum, thalamus, hippocampus dentate gyrus, substantia nigra, pons, medulla and cerebellum cortex. FTLD-TDP type B without MND and type D are not analysed in this study.

The samples were loaded on 15% SDS–PAGE gels. Proteins in the gel were then transferred onto a polyvinylidene difluoride membrane (Millipore). After blocking with 3% gelatine in 0.01 M PBS (pH 7.4), membranes were incubated overnight with phosphorylation dependent anti-TDP-43 rabbit polyclonal antibody (pS409/410, 1:1000; Hasegawa *et al.*, 2008), phosphorylation independent TDP-43 polyclonal antibody 10782-1-AP (TDP-43 pAb, 1:3000) and TDP-43 monoclonal antibody, 60019-2-Ig (TDP-43 mAb, 1:3000) (ProteinTech Group). After incubation with the appropriate biotinylated secondary antibody, immunolabelling was detected using the VECTASTAIN® ABC system (Vector Laboratories) coupled with a 3,3′-diaminobenzidine reaction intensified with nickel chloride. The blot membranes were digitally analysed, and densitometric analyses were performed with ImageJ version 1.44p (NIH, http://rsbweb.nih.gov/ij/index.html). The densitometry data were averaged for all cases in each group to illustrate the different patterns.

Immunohistochemistry

After cryoprotection in 15% sucrose in 0.01 M PBS (pH 7.4), paraformaldehyde-fixed tissue blocks were cut on a freezing microtome at 30-μm thickness. The free-floating sections were immunostained with phosphorylation-dependent TDP-43 monoclonal antibody (pS409/410, 1:10 000) (Inukai *et al.*, 2008) for 72 h in the cold. After treatment with mouse secondary antibody, immunolabelling was detected using the VECTASTAIN ®ABC system coupled with a 3,3′-diaminobenzidine reaction to yield a brown precipitate. Sections were lightly counterstained with heamatoxylin.

Protease treatment of phosphorylated TDP-43

Sarkosyl-insoluble fractions extracted from the neocortical regions of patients with ALS or FTLD-TDP were treated with final concentration of 100 μg/ml trypsin (Promega) or 10 μg/ml chymotrypsin (Sigma-Aldrich) at 37°C for 30 min. The reaction was stopped by boiling for 5 min. After centrifuging at 15 000 rpm for 1 min, the samples were analysed by immunoblotting as described earlier.

Mass spectrometry

Sarkosyl-insoluble, trypsin-resistant fractions were loaded on 15% SDS–PAGE gels. The pS409/410-positive ~16 kDa bands were dissected and digested in-gel with chymotrypsin. The digests were applied to the Paradigm MS4 high-performance liquid chromatography system (Microm BioResources). A reversed phase capillary column (Develosil ODS-HG5, 0.075 × 150 mm, Nomura Chemical) was used at a flow rate of 300 nl/min with a 4–80% linear gradient of acetonitrile in 0.1% formic acid. Eluted peptides were directly detected with an ion trap mass spectrometer, LXQ (Thermo Fisher Scientific). The obtained spectra were analysed with Mascot (Matrix Science).

Statistical analysis

The *P*-values for the description of the statistical significance of differences were calculated by means of the paired, two-tailed *t*-test using Prism 5.04 software (GraphPad Software, Inc).

Results

Banding patterns of phosphorylated C-terminal TDP-43 in ALS and FTLD with TDP-43 pathology

Immunoblot analysis using an antibody specific for abnormal TDP-43, pS409/410, showed high-molecular-weight smearing substances, phosphorylated full-length TDP-43 at 45 kDa and several C-terminal fragments at 18–26 kDa to be present in affected brain regions in all cases (Fig. 1). Three major bands at 23, 24 and 26 kDa, and two minor bands at 18 and 19 kDa were seen in the precentral gyrus and frontal cortex of cases with ALS, with the 24 kDa band being the most intense (Fig. 1A and F). In the lumbar spinal cord, the two minor bands at 18 and 19 kDa were barely present, but the banding pattern of the three major bands at 23, 24 and 26 kDa was similar to that in the cerebral cortex (Fig. 1A). No such pS409/410-positive TDP-43 bands were detected in control cases with Alzheimer's disease with no TDP-43 pathology (Fig. 1B). In the FTLD-TDP cases, the banding pattern could be distinguished into three types according to the FTLD-TDP histological subtype (Fig. 1C–E). In FTLD-TDP type A, three major bands at 23, 24 and 26 kDa, and two minor bands at 18 and 19 kDa were detected, with the 23 kDa band being the most intense (Fig. 1C and F). In FTLD-type B cases, the banding pattern was the same as that in the ALS cases (Fig. 1D and F). In FTLD-TDP type C cases, two major bands at 23 and 24 kDa, and two minor bands at 18 and 19 kDa were detected, with the 24 kDa band being the most intense, and the band at 26 kDa being hardly detectable (Fig. 1E and F). Densitometric analyses of the immunoblots for all cases are shown in Supplementary Fig. 1. Each component of the C-terminal fragments was significantly different (Fig. 1F).

Immunoblot analysis using phosphorylation independent TDP-43 polyclonal and monoclonal antibodies detected phosphorylated full-length TDP-43 at 45 kDa, two bands ~25 kDa and high-molecular-weight smears, in addition to the normal TDP-43 band at 43 kDa in ALS and various subtypes of FTLD-TDP. The banding patterns between ALS and various subtypes of FTLD-TDP could not be distinguished with these antibodies. In the cases with Alzheimer's disease, the normal TDP-43 band at 43 kDa was detected, but neither the phosphorylated 45 kDa band nor the ~25 kDa fragments were observed (Supplementary Fig. 2). Immunoblot analysis of α-tubulin in Tris saline-soluble fractions from cases with types A, B and C pathology showed no correlation between the banding pattern of α-tubulin and that of TDP-43 (Supplementary Fig. 3), indicating that the differences in the banding patterns are not because of protein degradation caused by a long post-mortem interval or unfavourable agonal status.

Immunohistochemistry and immunoblot analyses of phosphorylated TDP-43 in multiple regions of ALS and FTLD with TDP-43 pathology

In ALS cases, the neuronal cytoplasmic pathology, which included skein-like inclusions, irregularly shaped TDP-immunoreactive neuronal cytoplasmic inclusions and densely staining granules, was confirmed in multiple regions by immunohistochemistry analysis using pS409/410 (Fig. 2A–G). Glial cytoplasmic inclusions were also present in many regions. Glial cytoplasmic inclusions were more frequent in the white matter than in the grey matter (Fig. 2H). A few neuronal cytoplasmic inclusions were found in the cerebellar cortex granule cells (Fig. 2G). In FTLD-TDP type C, dystrophic neurites were seen in multiple regions except for the cerebellar cortex (Fig. 2I–O), whereas neuronal cytoplasmic inclusions were also present in the striatum and hippocampus dentate gyrus granule cells (Fig. 2J and L). No abnormal structures were found in the cerebellar cortex (data not shown). These observations show that pathological TDP-43 is present throughout many CNS areas in ALS, suggesting that ALS does not selectively affect only the motor system, but it is rather a multisystem neurodegenerative TDP-43 proteinopathy.

Immunoblot analyses of three ALS cases confirmed that phosphorylated TDP-43 and the C-terminal fragments are deposited in multiple brain regions in ALS (Fig. 3A). Relatively strong immunoreactivities were detected in the striatum (in Cases 3 and 5) and substantia nigra (in Cases 1 and 5), although this varied between cases (Fig. 3A). Importantly, the banding pattern for the TDP-43 C-terminal fragments in these three cases was basically the same in all brain regions examined (Fig. 3A). In FTLD-TDP type C, a C-terminal banding pattern, clearly distinct from that

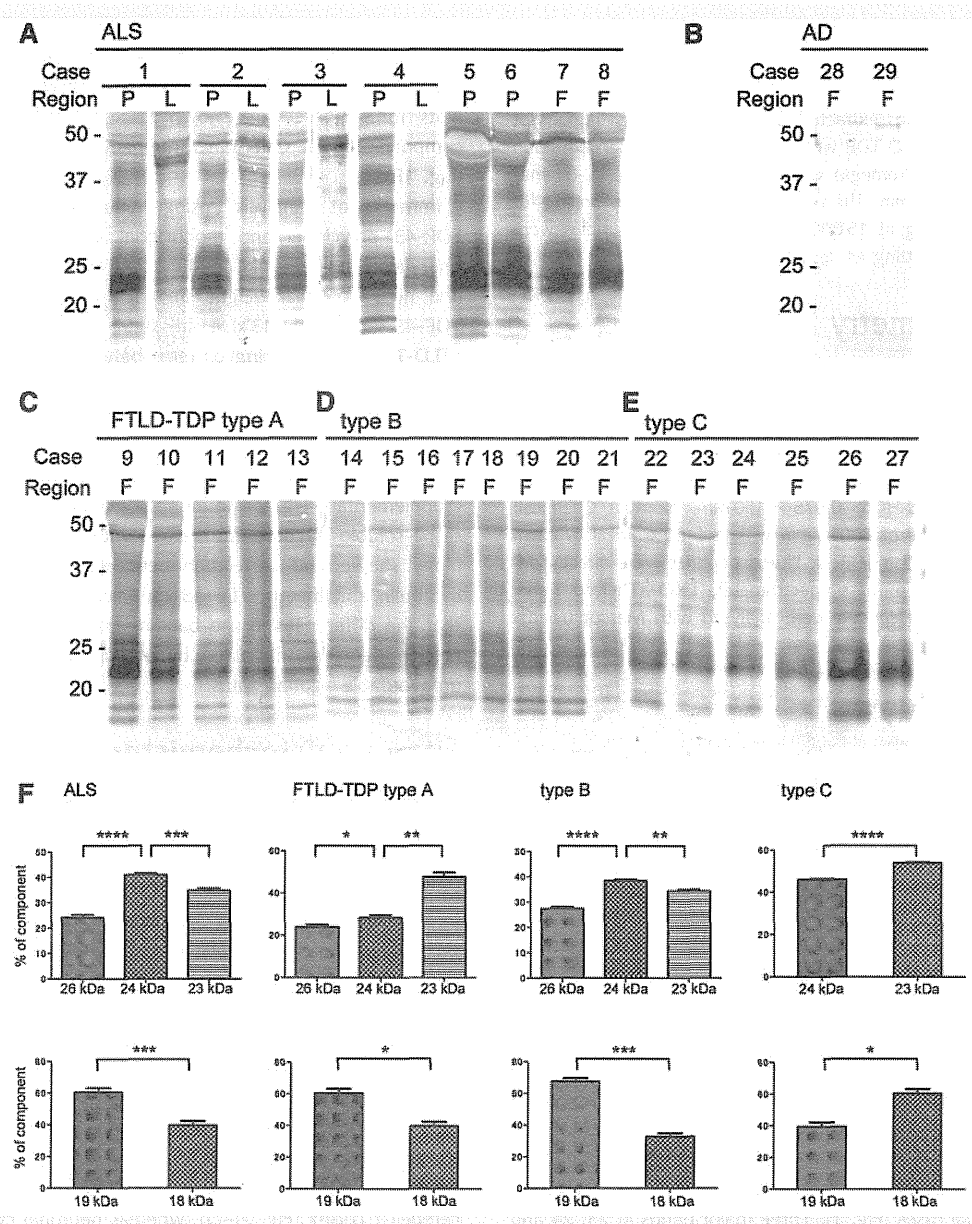

Figure 1 Immunoblot analyses of sarkosyl-insoluble TDP-43 in the brains or spinal cords of ALS (Cases 1–8) (**A**), Alzheimer's disease (Cases 28–29) (**B**), FTLD-TDP type A (Cases 9–13) (**C**), FTLD-TDP type B (Cases 14–21) (**D**) and FTLD-TDP type C (Cases 22–27) (**E**), using a phosphorylation-dependent anti-TDP-43 antibody (pS409/410). In all cases, high-molecular-weight smearing substances, phosphorylated full-length TDP-43 at 45 kDa and several C-terminal fragments at 18–26 kDa are detected. In ALS (**A**) and FTLD-TDP type B (**D**) cases, three major bands at 23, 24 and 26 kDa and two minor bands at 18 and 19 kDa are detected, whereas in the FTLD-TDP Type C (**E**) cases, two major bands at 23 and 24 and two minor bands at 18 and 19 kDa. A 24 kDa band is the most intense in ALS (**A**) and FTLD-TDP type B (**E**), whereas a 23 kDa band is the most intense in FTLD-TDP type C (**D**). The band pattern of the cases with type A (**C**) is an intermediate between FTLD-TDP type B (**D**) and FTLD-TDP type C (**E**). In spinal cords of cases with ALS, the 18 and 19 kDa bands are hardly detectable, but the same banding pattern of the 23–26 kDa bands as in precentral gyrus is detected. No such TDP-43 fragments are detected in brains of patients with Alzheimer's disease (AD) (**B**). The intensity of each C-terminal band was analysed using the ImageJ software and each component was statistically analysed by Student's *t*-test (**F**). Data indicate mean (SEM). $^{****}P < 0.0001$, $^{***}P < 0.001$, $^{**}P < 0.01$, $^{*}P < 0.05$. F = frontal cortex; L = lumbar part of spinal cord; P = precentral cortex.

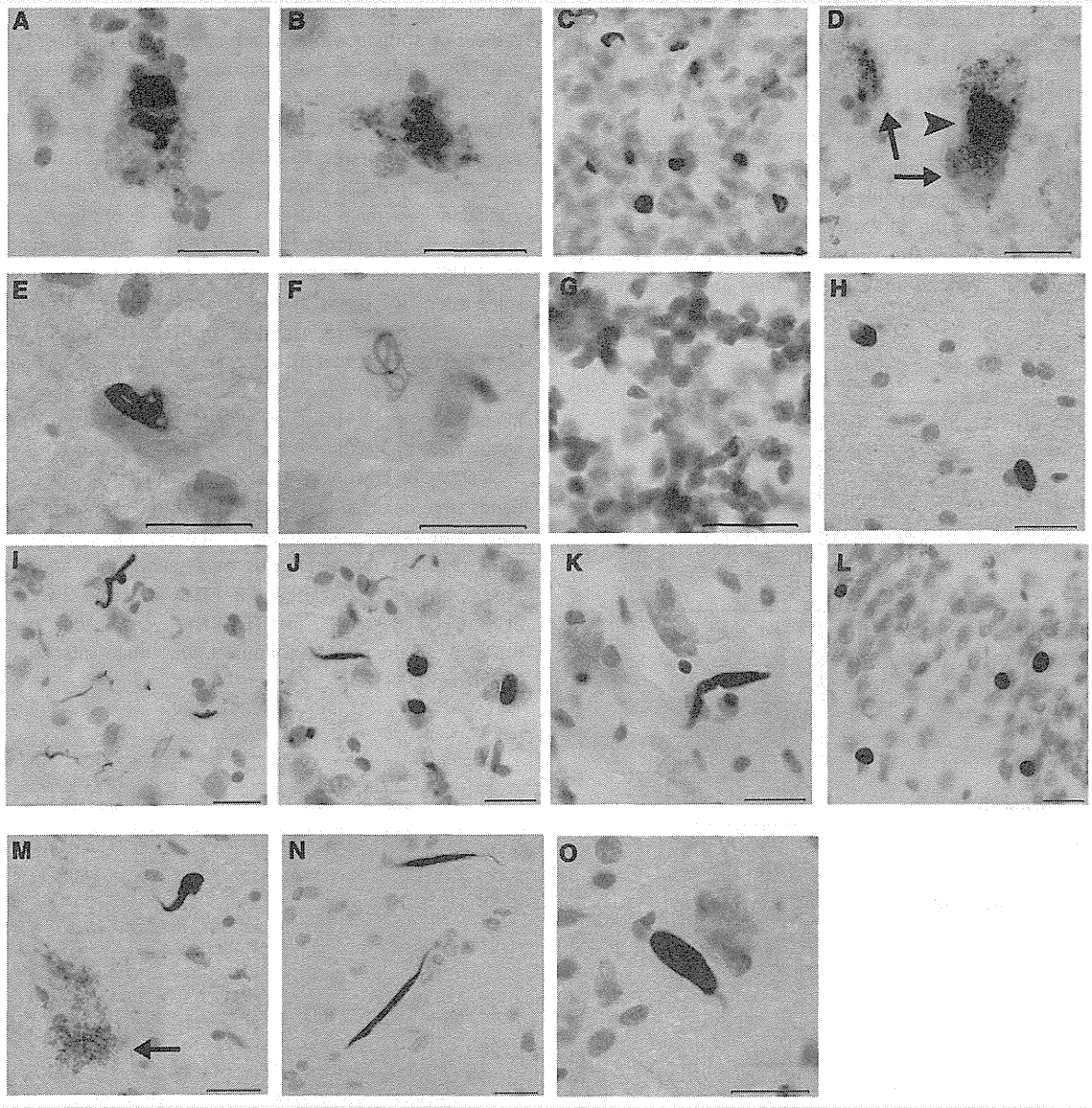

Figure 2 Phosphorylated TDP-43-positive structures observed in different brain regions and spinal cords of ALS (**A–H**) and FTLD-type C (**I–O**) using a phosphorylation-dependent anti-TDP-43 antibody (pS409/410). (**A**) Lewy body-like inclusion in the striatum neuron. (**B**) Cytoplasmic granular staining in the thalamus. (**C**) Neuronal cytoplasmic inclusions in the granular cells of hippocampus. (**D**) Irregularly shaped TDP-immunoreactive neuronal cytoplasmic inclusion in the substantia nigra (arrowhead). The arrows denote neuromelanin granules. (**E**) Skein-like inclusion in the motor nucleus of trigeminal nerve of pons. (**F**) Skein-like inclusion in the inferior olivary nucleus of medulla. (**G**) Neuronal cytoplasmic inclusion in the granular cells of cerebellar cortex. (**H**) Glial cytoplasmic inclusions in the white matter of precentral cortex. (**I**) Dystrophic neurites in the temporal cortex, (**J**) dystrophic neurites and neuronal cytoplasmic inclusions in the striatum. (**K**) Dystrophic neurites in the thalamus. (**L**) Neuronal cytoplasmic inclusions in the granular cells of hippocampus. (**M**) Dystrophic neurites in the substantia nigra. The arrow denotes neuromelanin granules. (**N**) Dystrophic neurites in the pons. (**O**) Dystrophic neurites in the *medullary reticular formation. Scale bars* = 20 μm.

of ALS, was detected in the temporal cortex, striatum and hippocampus, but was barely detected in the thalamus, substantia nigra, pons and medulla, and not at all in the cerebellar cortex (Fig. 3B). The banding pattern observed in these brain regions was indistinguishable (Fig. 3B). These results suggest that the same abnormal TDP-43 molecular species is deposited in different brain regions and different cell types, although the morphology of the TDP-43 inclusions may be different in the brain regions. Densitometric analyses of the immunoblots for all cases are shown in Supplementary Fig. 4.

Protease-resistant TDP-43 in ALS and FTLD with frontotemporal dementia-43 pathology

These different banding patterns in TDP-43 proteinopathies may represent different conformations of abnormal TDP-43 or their aggregates. To test this hypothesis, we subjected the abnormal TDP-43 recovered in the sarkosyl-insoluble pellets to protease treatment and analysed the protease-resistant bands. Proteins can be easily cleaved by proteases if they are denatured or unstructured, but domains that have rigid structures, such as a β-sheet conformation or that are structurally buried or interacting with other molecules, are highly resistant to proteases. On trypsin or chymotrypsin treatment, the full-length 45-kDa band and the smearing substance of TDP-43 disappeared, leaving protease-resistant fragments at 16–25 kDa (Figs 4 and 5). As expected, the protease-resistant banding patterns were different and distinguishable into three patterns (Figs 4 and 5). In ALS, trypsin-resistant doublet bands at 16 and 15 kDa, and two minor bands at ~24 kDa were detected, whereas a single band at 16 kDa and some additional bands at ~24 kDa were detected in FTLD-TDP type A (Fig. 4A, Lanes 1 and 2). In FTLD-TDP type B, the same banding pattern as that in ALS was observed (Fig. 4A, Lane 3). In FTLD-TDP type C, a broad single band at 16 kDa and some additional bands at ~24 kDa were detected (Fig. 4A, Lane 4). No such bands were detected in Alzheimer's disease (Fig. 4A, Lane 5).

Similarly, on chymotrypsin treatment, multiple protease-resistant bands were detected at 16–25 kDa and the chymotrypsin-resistant band patterns were also different between the three disease subtypes (Fig. 4B). Doublet bands were seen in ALS and FTLD-TDP type B, but only a single band in FTLD-TDP type C was detected at ~16 kDa (Fig. 4B). In FTLD-TDP type A, the lower band (15 kDa) of the ~16 kDa doublet was more intense than the upper one (16 kDa).

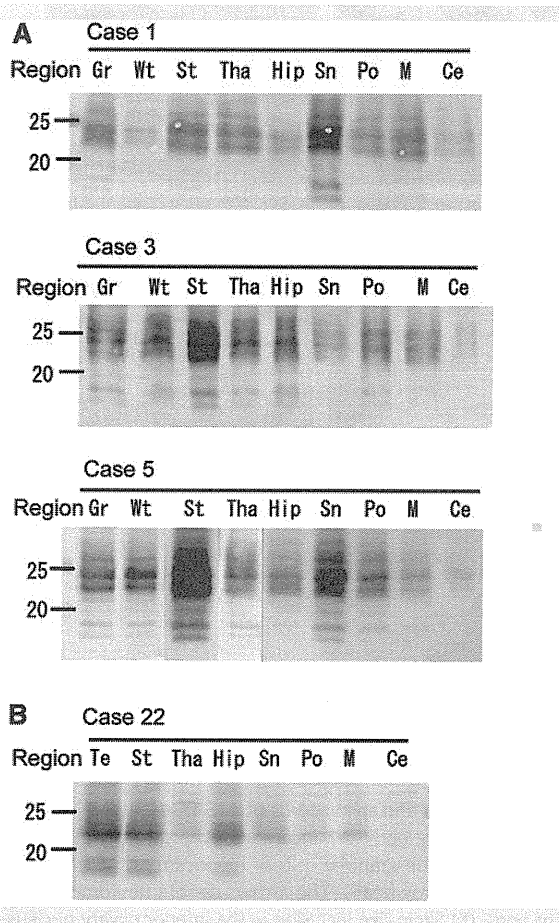

Figure 3 Immunoblot analyses of the C-terminal fragments of phosphorylated TDP-43 in the different brain regions of cases with ALS (Cases 1, 3 and 5, as shown in Fig. 1) (**A**) and FTLD-type C (Case 22, as shown in Fig. 1) (**B**). (**A**) Immunoblots of insoluble TDP-43 in the grey or white matter of precentral cortex, striatum, thalamus, hippocampus, substantia nigra, pons and medulla of ALS cases. (**B**) Immunoblot of TDP-43 in temporal cortex, striatum, hippocampus, thalamus, substantia nigra, pons and cerebellar cortex of the case with FTLD-TDP type C. Ce = Cerebellar cortex; Gr = grey matter of precentral gyrus; Hip = hippocampus; M = medulla; Po = pons; Sn = substantia nigra; St = striatum; Tha = thalamus; Te = temporal cortex; Wt = white matter of precentral gyrus. Immunoblots of spinal cords of cases with ALS are shown in Fig. 1.

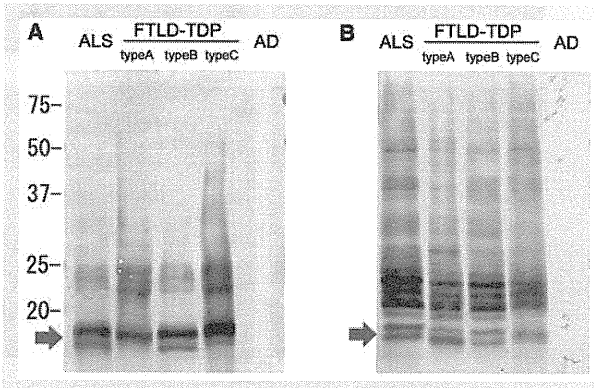

Figure 4 Immunoblot analysis of phosphorylated TDP-43 from representative ALS and FTLD-TDP cases after protease treatment. (**A**) Immunoblot of insoluble TDP-43 from cases with ALS, FTLD-TDP type A, type B, type C and Alzheimer's disease (AD) after trypsin treatment. Doublet bands at ~16 kDa (arrow) and some minor 23–24 kDa bands are detected in ALS and FTLD-TDP type B, whereas a single band at ~16 kDa and several bands at 23 and 24 kDa are detected in FTLD-TDP type A and type C. No such bands are detected in the Alzheimer's disease case. (**B**) Immunoblot of insoluble TDP-43 from cases with ALS, FTLD-TDP type A, type B, type C and Alzheimer's disease after chymotrypsin treatment. Multiple protease-resistant TDP-43 bands are detected at 16–25 kDa. Doublet bands at ~16 kD (arrow) are detected in ALS and FTLD-TDP type A and B, whereas a single band at ~16 kD (arrow) is detected in the case with FTLD-TDP type C. In FTLD-TDP type A, the lower band of the doublet at 16 kDa is more intense. No such bands are detected in the Alzheimer's disease case.

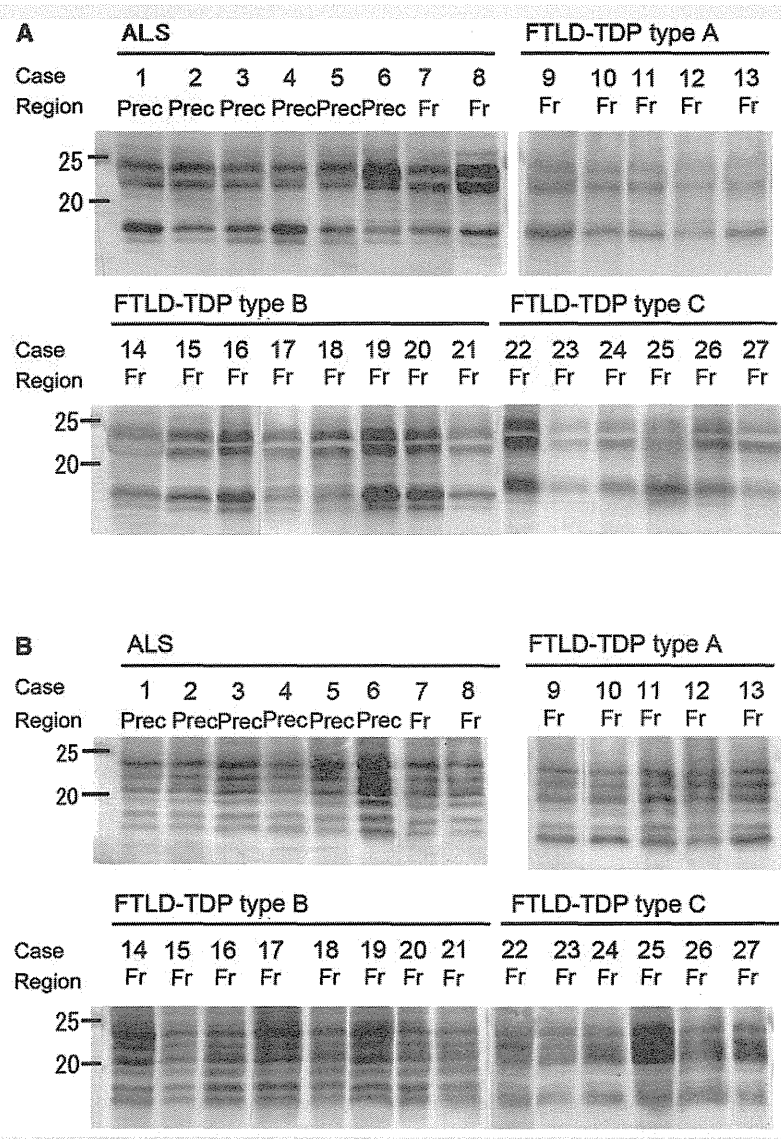

Figure 5 *Comparison of the protease-resistant TDP-43 banding patterns in ALS and FTLD-TDP. Immunoblot analyses of trypsin-resistant* (**A**) and chymotrypsin-resistant (**B**) fragments of TDP-43 from all cases examined. The banding patterns of ALS and FTLD-TDP type B cases are indistinguishable. Fr = frontal cortex; Prec = precentral gyrus.

In all cases examined, the trypsin-resistant banding patterns were clearly distinguishable between the disease subtypes in accordance with the three different types of banding pattern of TDP-43 C-terminal fragments, although it is difficult to distinguish the trypsin band pattern of type A from that of type C (Figs 5A, 6A and Supplementary Fig. 5). The chymotrypsin-resistant banding patterns were distinguishable and could be differentiated into three types (Figs 5B, 6B and Supplementary Fig. 6), also in accordance with the banding pattern of the TDP-43 C-terminal fragment. The banding patterns of ALS and FTLD-TDP type B were the same, whereas the banding pattern of FTLD-TDP type A was distinguishable from those of type C and type B (Figs 4 and 5). The combination analyses of trypsin and chymotrypsin-resistant banding patterns confirmed that TDP-43 proteinopathies can also be biochemically distinguishable into three types according to TDP-43 subtypes. These results strongly suggest that the different C-terminal banding patterns represent different conformations of TDP-43 aggregates and that the distinct types of TDP-43 are deposited in association with distinct pathological phenotypes of TDP-43 proteinopathies.

Immunoblot analysis using phosphorylation independent TDP-43 polyclonal and monoclonal antibodies detected some TDP-43 fragments in the ALS and FTLD-TDP cases after trypsin or chymotrypsin treatment, although no clear difference was observed in the banding patterns between ALS and other subtypes of FTLD-TDP (Supplementary Fig. 7). The distinctive

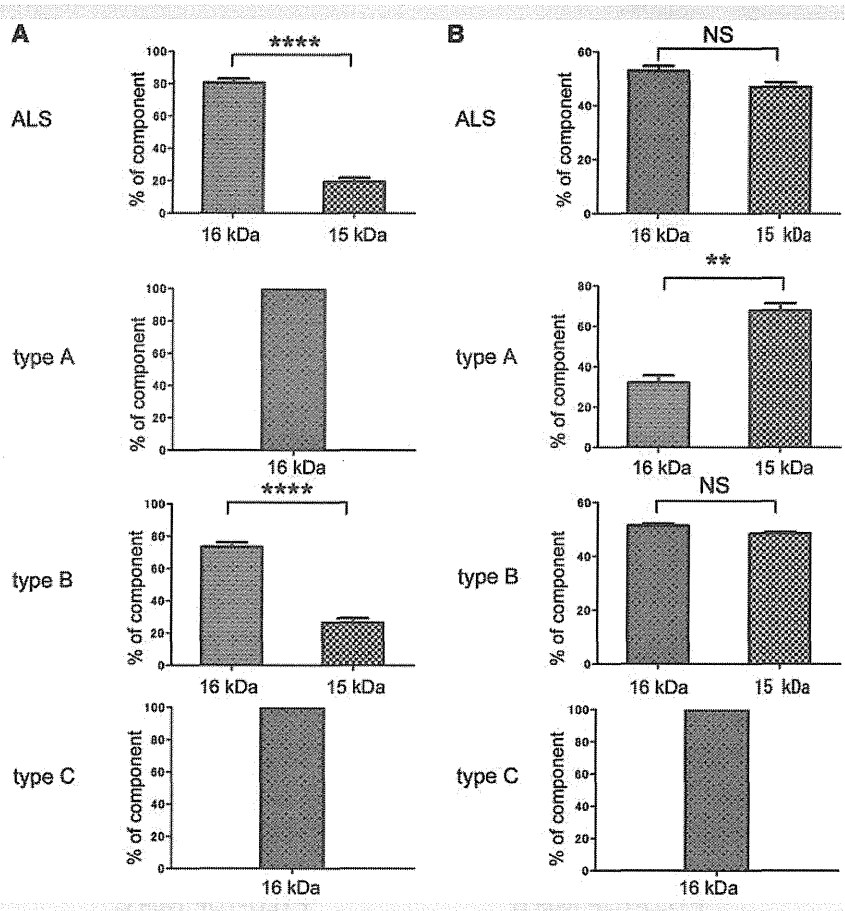

Figure 6 Quantitative analysis of protease-resistant ~16 kDa band. (**A**) The intensity of trypsin-resistant ~16 kDa band of each case was quantitated with ImageJ and statistically analysed. (**B**) The intensity of chymotrypsin-resistant ~16 kDa band of each case was quantitated with ImageJ and statistically analysed. Data indicate mean (SEM). ****$P < 0.0001$, **$P < 0.01$, NS = not significant.

protease-resistant bands at ~16 kDa of ALS were not detected with both phosphorylation independent antibodies (Supplementary Fig. 8).

We also analysed the banding pattern of phosphorylated TDP-43 in another series of five sporadic cases with TDP-43 pathology (Alzheimer's disease, Alzheimer's disease/dementia with Lewy bodies and Alzheimer's disease/argyrophilic grain disease) (Supplementary Table 1). The banding pattern of the C-terminal fragments, and trypsin- or chymotrypsin-resistant fragments, in these were same as those of FTLD-TDP type A with *GRN* mutation (Supplementary Fig. 9).

Mass spectrometric analysis of protease-resistant bands of TDP-43 in ALS and FTLD-TDP type C

To further investigate the differences in the abnormal TDP-43 protein species at a molecular level, we analysed the ~16 kDa trypsin-resistant bands by mass spectrometry. Mass analysis of chymotrypsin digests of ~16 kDa trypsin-resistant fragments identified 4 peptides, amino acid residues 277–289, 290–299, 294–333 and 300–316, suggesting these peptides are derived from trypsin-resistant fragments 276–414 and 294–414. Mass spectrometric analysis of the single broad band from FTLD-TDP type C identified the peptides of amino acids 273–283, 277–289, 290–313 and 317–330, strongly suggesting that the trypsin-resistant fragments from FTLD-TDP type C are derived from peptides 273–414 and 276–414. These analyses clearly indicate that trypsin-resistant core regions of the abnormal TDP-43 accumulated in the brain are not necessarily the same between ALS and FTLD (Supplementary Fig. 10).

Discussion

In this study, we have shown that the banding patterns for TDP-43 C-terminal fragments in ALS and FTLD are distinguishable and classifiable into at least three types. This difference was consistently demonstrated in 27 cases, eight with ALS, five with FTLD-TDP type A, eight with FTLD-TDP type B and six with FTLD-TDP type C. These results strongly suggest that distinct

types of TDP-43 molecules constitute the distinct types of pathologies of TDP-43 and determine the clinicopathological phenotypes of TDP-43 proteinopathies. In TDP-43 histopathology, ALS is considered to represent a distinct pathological subtype because the distribution of TDP-43 inclusions is different from that of FTLD-TDP (Mackenzie *et al.*, 2006a). However, as shown in this study, the TDP-43 accumulations in ALS and FTLD-TDP type B are biochemically indistinguishable. In fact, clinical and histopathological motor neuron disease is often present in cases with FTLD-TDP type B histology. In the three types of phosphorylated C-terminal TDP-43 banding pattern, the pattern seen in FTLD-TDP type C is the most distinctive, lacking the 26 kDa band detected in ALS, FTLD-TDP type A and type B cases (Fig. 1). The clinical diagnosis of the FTLD-TDP type C cases was semantic dementia in every instance, consistent with other studies showing this type of histology to be associated with semantic dementia (Mackenzie *et al.*, 2006a). FTLD is clinically classified into frontotemporal dementia, demantic dementia and progressive non-fluent aphasia, based on topographical distributions of degeneration (Neary *et al.*, 1998). In frontotemporal dementia, the bilateral frontal and temporal lobes are affected, whereas the bilateral temporal lobes are affected in semantic dementia and the left hemisphere in progressive non-fluent aphasia. Present data showing the most distinctive pattern of abnormal TDP-43 in type C indicate that semantic dementia may be biochemically different from frontotemporal dementia. Similar differences in tau fragment banding patterns have been shown between progressive supranuclear palsy and corticobasal degeneration (Arai *et al.*, 2004). Progressive supranuclear palsy and corticobasal degeneration are neurodegenerative diseases that are characterized by intracytoplasmic aggregates of hyperphosphorylated tau with four microtubule-binding repeats, with distinctive pathological features. Immunoblot analysis of Sarkosyl-insoluble tau demonstrated that a 33 kDa C-terminal fragment of tau band predominated in progressive supranuclear palsy, whereas two closely related bands of ~37 kDa predominated in corticobasal degeneration. The clinicopathological subtypes of these diseases may be explained by different conformations of protein aggregates or species of abnormal proteins.

Unfortunately, we were unable to obtain brain tissue samples from patients with FTLD-TDP type D (associated with *VCP* mutation; Cairns *et al.*, 2007b; Neumann *et al.*, 2007). However, because the deposition of abnormal TDP-43 in this disorder is mostly within neuronal nuclei, it is possible that the conformation of abnormal TDP-43 in FTLD-TDP type D may also differ from that in FTLD-TDP types A–C. Familial ALS and FTLD-TDP cases in which known mutations [*GRN* (Baker *et al.*, 2006) or *C9ORF72* (DeJesus-Hernandez *et al.*, 2011; Renton *et al.*, 2011)] were examined in this study. In FTLD-TDP due to *GRN* mutations, type A pathology is exclusively seen (Mackenzie *et al.*, 2006b; Cairns *et al.*, 2007b; Josephs *et al.*, 2007). All our cases with FTLD with *GRN* mutation showed the same C-terminal banding patterns of phosphorylated TDP-43 corresponding to type A histology. Some recent studies describing the clinical and pathological features of cases of FTLD-TDP with hexanucleotide repeat expansions in *C9ORF72* reported that many of the 'pure' frontotemporal dementia cases had type A pathology, whereas many of the combined frontotemporal dementia and motor neuron disease cases had type B pathology (Murray *et al.*, 2011; Boeve *et al.*, 2012; Hsiung *et al.*, 2012; Mahoney *et al.*, 2012; Simon-Sanchez *et al.*, 2012; Snowden *et al.*, 2012). Present cases with *C9ORF72* expansions included one case of ALS, one case of pure frontotemporal dementia with type A pathology, and two cases of frontotemporal dementia with motor neuron disease and type B pathology. The C-terminal banding pattern of these cases with familial ALS and frontotemporal dementia with motor neuron disease was not different from that in the sporadic ALS and FTLD-TDP type B cases, and that of the frontotemporal dementia case was not different from that in the cases with *GRN* mutation. Therefore, expansions in *C9ORF72* do not seem to influence the various types of TDP-43 C-terminal banding pattern or histological type of TDP-43 pathology.

Immunohistochemical studies using TDP-43 antibodies have shown that pathological TDP-43 is present throughout many CNS areas in ALS, suggesting that ALS does not selectively affect only the motor system, but is rather a multisystem neurodegenerative TDP-43 proteinopathy (Geser *et al.*, 2008). We also confirmed this viewpoint, immunohistochemically and biochemically, finding the same disease characteristic C-terminal fragment (banding) patterns of phosphorylated TDP-43 within the cerebral cortex, spinal cord and the other different brain regions in ALS. Although the types of pathological structures or their morphologies detected on immunohistochemistry analysis appeared different, the banding patterns for the C-terminal fragments were the same in all regions examined in three patients with ALS. This was also true for the one case with FTLD-TDP type C, where the same banding pattern of the C-terminal fragments was detected in several different brain regions beyond the frontal cortex (Fig. 3). These results strongly suggest that the same abnormal TDP-43 molecule is deposited in different brain regions in ALS (and probably also in FTLD-TDP type B) and FTLD-TDP type C, although we need to examine whether this is also true for cases with FTLD-TDP type A. Importantly, the extent of the abnormal protein pathology is closely correlated with the disease progression, such as Alzheimer's disease in tauopathies (Braak and Braak, 1991), and Parkinson's disease in α-synucleinopathies (Braak *et al.*, 2003; Saito *et al.*, 2003). However, the molecular mechanisms governing different clinicopathological phenotypes of these neurodegenerative diseases and their progression are poorly understood. Recent studies using cellular or animal models have suggested that aggregation-prone proteins, such as tau and α-synuclein, can spread to other cells and brain regions like prion disorders (Clavaguera *et al.*, 2009; Frost *et al.*, 2009; Nonaka *et al.*, 2010). The spreading of α-synuclein lesions to the grafts is also observed in Parkinson's disease brains after transplantation (Li *et al.*, 2008). However, it remains to be clarified whether the 'propagating' abnormal protein species represents a distinct 'strain type' that can be differentiated by molecular criteria in human patients or whether the species are the same in different brain regions.

We have also shown that the banding patterns of protease-resistant fragments of phosphorylated TDP-43 are similarly different in accordance with the banding patterns seen in untreated C-terminal fragments, confirming the direct link between neuropathological subtypes and biochemical banding patterns. The mass spectrometric analysis indicated that the protease resistant regions

of abnormal TDP-43 are different between the diseases. As abnormally phosphorylated TDP-43 has been shown to accumulate in a filamentous form in ALS spinal cords (Hasegawa *et al.*, 2008), the filament core regions may be different between the diseases. Protease-resistant bands, and differences in banding patterns, have been reported in the prion diseases, Creutzfeldt–Jakob disease and bovine spongiform encephalopathy (Collinge *et al.*, 1996). Protease-resistant prion protein extracted from cases with new-variant Creutzfeldt–Jakob disease showed a different and characteristic pattern from that in cases with sporadic Creutzfeldt–Jakob disease, with the banding pattern being indistinguishable from that of mice infected with bovine spongiform encephalopathy prion. Protease-treated prion protein species are thought to have different mobilities because of different conformations. These observations in prion disease suggest that the different banding patterns to the abnormal TDP-43 fragments in ALS and FTLD might represent different TDP-43 strains with different conformations.

Recently, TDP-43 pathology has been detected in some cases with Alzheimer's disease (Arai *et al.*, 2009). We have shown here that the banding patterns of TDP-43 in cases of Alzheimer's disease with TDP-43 pathology are the same as those in FTLD-TDP type A. These novel observations suggest a biochemical commonality between FTLD and Alzheimer's disease with respect to TDP-43 pathology.

The results shown in this study also suggest a molecular basis for the clinicopathological classification of TDP-43 proteinopathies, which complements the histological classifications (Mackenzie *et al.*, 2011).

Funding

This work was supported by a Grant-in-Aid for Scientific Research (A) (to M.H., 11000624) from Ministry of Education, Culture, Sports, Science and Technology of Japan, and grants from Ministry of Health, Labor and Welfare of Japan (to M.H.).

Supplementary material

Supplementary material is available at *Brain* online.

References

Arai T, Mackenzie IR, Hasegawa M, Nonoka T, Niizato K, Tsuchiya K, et al. Phosphorylated TDP-43 in Alzheimer's disease and dementia with Lewy bodies. Acta Neuropathol (Berl) 2009; 117: 125–36.

Arai T, Hasegawa M, Akiyama H, Ikeda K, Nonaka T, Mori H, et al. TDP-43 is a component of ubiquitin-positive tau-negative inclusions in frontotemporal lobar degeneration and amyotrophic lateral sclerosis. Biochem Biophys Res Commun 2006; 351: 602–11.

Arai T, Ikeda K, Akiyama H, Nonaka T, Hasegawa M, Ishiguro K, et al. Identification of amino-terminally cleaved tau fragments that distinguish progressive supranuclear palsy from corticobasal degeneration. Ann Neurol 2004; 55: 72–9.

Armstrong RA, Ellis W, Hamilton RL, Mackenzie IR, Hedreen J, Gearing M, et al. Neuropathological heterogeneity in frontotemporal lobar degeneration with TDP-43 proteinopathy: a quantitative study of 94 cases using principal components analysis. J Neural Transm 2010; 117: 227–39.

Baker M, Mackenzie IR, Pickering-Brown SM, Gass J, Rademakers R, Lindholm C, et al. Mutations in progranulin cause tau-negative frontotemporal dementia linked to chromosome 17. Nature 2006; 442: 916–19.

Boeve BF, Boylan KB, Graff-Radford NR, Dejesus-Hernandez M, Knopman DS, Pedraza O, et al. Characterization of frontotemporal dementia and/or amyotrophic lateral sclerosis associated with the GGGGCC repeat expansion in *C9ORF72*. Brain 2012; 135: 765–83.

Braak H, Braak E. Neuropathological stageing of Alzheimer-related changes. Acta Neuropathol 1991; 82: 239–59.

Braak H, Del Tredici K, Rub U, de Vos RA, Jansen Steur EN, Braak E. Staging of brain pathology related to sporadic Parkinson's disease. Neurobiol Aging 2003; 24: 197–211.

Brooks BR. El Escorial World Federation of Neurology criteria for the diagnosis of amyotrophic lateral sclerosis. Subcommittee on Motor Neuron Diseases/Amyotrophic Lateral Sclerosis of the World Federation of Neurology Research Group on Neuromuscular Diseases and the El Escorial "Clinical limits of amyotrophic lateral sclerosis" workshop contributors. J Neurol Sci 1994; 124 (Suppl): 96–107.

Cairns NJ, Bigio EH, Mackenzie IR, Neumann M, Lee VM, Hatanpaa KJ, et al. Neuropathologic diagnostic and nosologic criteria for frontotemporal lobar degeneration: consensus of the Consortium for Frontotemporal Lobar Degeneration. Acta Neuropathol 2007a; 114: 5–22.

Cairns NJ, Neumann M, Bigio EH, Holm IE, Troost D, Hatanpaa KJ, et al. TDP-43 in familial and sporadic frontotemporal lobar degeneration with ubiquitin inclusions. Am J Pathol 2007b; 171: 227–40.

Clavaguera F, Bolmont T, Crowther RA, Abramowski D, Frank S, Probst A, et al. Transmission and spreading of tauopathy in transgenic mouse brain. Nat Cell Biol 2009; 11: 909–13.

Collinge J, Sidle KC, Meads J, Ironside J, Hill AF. Molecular analysis of prion strain variation and the aetiology of 'new variant' CJD. Nature 1996; 383: 685–90.

DeJesus-Hernandez M, Mackenzie IR, Boeve BF, Boxer AL, Baker M, Rutherford NJ, et al. Expanded GGGGCC hexanucleotide repeat in noncoding region of *C9ORF72* causes chromosome 9p-linked FTD and ALS. Neuron 2011; 72: 245–56.

Frost B, Jacks RL, Diamond MI. Propagation of tau misfolding from the outside to the inside of a cell. J Biol Chem 2009; 284: 12845–52.

Geser F, Brandmeir NJ, Kwong LK, Martinez-Lage M, Elman L, McCluskey L, et al. Evidence of multisystem disorder in whole-brain map of pathological TDP-43 in amyotrophic lateral sclerosis. Arch Neurol 2008; 65: 636–41.

Geser F, Martinez-Lage M, Robinson J, Uryu K, Neumann M, Brandmeir NJ, et al. Clinical and pathological continuum of multisystem TDP-43 proteinopathies. Arch Neurol 2009; 66: 180–9.

Gitcho MA, Bigio EH, Mishra M, Johnson N, Weintraub S, Mesulam M, et al. TARDBP 3'-UTR variant in autopsy-confirmed frontotemporal lobar degeneration with TDP-43 proteinopathy. Acta Neuropathol 2009; 118: 633–45.

Hasegawa M, Arai T, Nonaka T, Kametani F, Yoshida M, Hashizume Y, et al. Phosphorylated TDP-43 in frontotemporal lobar degeneration and amyotrophic lateral sclerosis. Ann Neurol 2008; 64: 60–70.

Hsiung GY, Dejesus-Hernandez M, Feldman HH, Sengdy P, Bouchard-Kerr P, Dwosh E, et al. Clinical and pathological features of familial frontotemporal dementia caused by *C9ORF72* mutation on chromosome 9p. Brain 2012; 135: 709–22.

Inukai Y, Nonaka T, Arai T, Yoshida M, Hashizume Y, Beach TG, et al. Abnormal phosphorylation of Ser409/410 of TDP-43 in FTLD-U and ALS. FEBS Lett 2008; 582: 2899–904.

Josephs KA, Ahmed Z, Katsuse O, Parisi JF, Boeve BF, Knopman DS, et al. Neuropathologic features of frontotemporal lobar degeneration with ubiquitin-positive inclusions with progranulin gene (*GRN*) mutations. J Neuropathol Exp Neurol 2007; 66: 142–51.

Kabashi E, Valdmanis PN, Dion P, Spiegelman D, McConkey BJ, Vande Velde C, et al. TARDBP mutations in individuals with sporadic and familial amyotrophic lateral sclerosis. Nat Genet 2008; 40: 572–4.

Kovacs GG, Murrell JR, Horvath S, Haraszti L, Majtenyi K, Molnar MJ, et al. TARDBP variation associated with frontotemporal dementia, supranuclear gaze palsy, and chorea. Mov Disord 2009; 24: 1843–7.

Li JY, Englund E, Holton JL, Soulet D, Hagell P, Lees AJ, et al. Lewy bodies in grafted neurons in subjects with Parkinson's disease suggest host-to-graft disease propagation. Nat Med 2008; 14: 501–3.

Mackenzie IR, Baborie A, Pickering-Brown S, Du Plessis D, Jaros E, Perry RH, et al. Heterogeneity of ubiquitin pathology in frontotemporal lobar degeneration: classification and relation to clinical phenotype. Acta Neuropathol 2006a; 112: 539–49.

Mackenzie IR, Baker M, Pickering-Brown S, Hsiung GY, Lindholm C, Dwosh E, et al. The neuropathology of frontotemporal lobar degeneration caused by mutations in the progranulin gene. Brain 2006b; 129: 3081–90.

Mackenzie IR, Neumann M, Baborie A, Sampathu DM, Du Plessis D, Jaros E, et al. A harmonized classification system for FTLD-TDP pathology. Acta Neuropathol 2011; 122: 111–13.

Mahoney CJ, Beck J, Rohrer JD, Lashley T, Mok K, Shakespeare T, et al. Frontotemporal dementia with the *C9ORF72* hexanucleotide repeat expansion: clinical, neuroanatomical and neuropathological features. Brain 2012; 135: 736–50.

Murray ME, DeJesus-Hernandez M, Rutherford NJ, Baker M, Duara R, Graff-Radford NR, et al. Clinical and neuropathologic heterogeneity of c9FTD/ALS associated with hexanucleotide repeat expansion in *C9ORF72*. Acta Neuropathol 2011; 122: 673–90.

Neary D, Snowden JS, Gustafson L, Passant U, Stuss D, Black S, et al. Frontotemporal lobar degeneration: a consensus on clinical diagnostic criteria. Neurology 1998; 51: 1546–54.

Neumann M, Mackenzie IR, Cairns NJ, Boyer PJ, Markesbery WR, Smith CD, et al. TDP-43 in the ubiquitin pathology of frontotemporal dementia with *VCP* gene mutations. J Neuropathol Exp Neurol 2007; 66: 152–7.

Neumann M, Sampathu DM, Kwong LK, Truax AC, Micsenyi MC, Chou TT, et al. Ubiquitinated TDP-43 in frontotemporal lobar degeneration and amyotrophic lateral sclerosis. Science 2006; 314: 130–3.

Nonaka T, Watanabe ST, Iwatsubo T, Hasegawa M. Seeded aggregation and toxicity of α-synuclein and tau: cellular models of neurodegenerative diseases. J Biol Chem 2010; 285: 34885–98.

Renton AE, Majounie E, Waite A, Simon-Sanchez J, Rollinson S, Gibbs JR, et al. A hexanucleotide repeat expansion in *C9ORF72* is the cause of chromosome 9p21-linked ALS-FTD. Neuron 2011; 72: 257–68.

Saito Y, Kawashima A, Ruberu NN, Fujiwara H, Koyama S, Sawabe M, et al. Accumulation of phosphorylated alpha-synuclein in aging human brain. J Neuropathol Exp Neurol 2003; 62: 644–54.

Simon-Sanchez J, Dopper EG, Cohn-Hokke PE, Hukema RK, Nicolaou N, Seelaar H, et al. The clinical and pathological phenotype of *C9ORF72* hexanucleotide repeat expansions. Brain 2012; 135: 723–35.

Snowden JS, Rollinson S, Thompson JC, Harris JM, Stopford CL, Richardson AM, et al. Distinct clinical and pathological characteristics of frontotemporal dementia associated with *C9ORF72* mutations. Brain 2012; 135: 693–708.

Sreedharan J, Blair IP, Tripathi VB, Hu X, Vance C, Rogelj B, et al. TDP-43 mutations in familial and sporadic amyotrophic lateral sclerosis. Science 2008; 319: 1668–72.

Tan CF, Eguchi H, Tagawa A, Onodera O, Iwasaki T, Tsujino A, et al. TDP-43 immunoreactivity in neuronal inclusions in familial amyotrophic lateral sclerosis with or without SOD1 gene mutation. Acta Neuropathol 2007; 113: 535–42.

Saito et al. Molecular Neurodegeneration 2012, 7:50
http://www.molecularneurodegeneration.com/content/7/1/50

MOLECULAR NEURODEGENERATION

RESEARCH ARTICLE Open Access

Hyperpolarization-activated cyclic nucleotide gated channels: a potential molecular link between epileptic seizures and Aβ generation in Alzheimer's disease

Yuhki Saito[1], Tsuyoshi Inoue[2], Gang Zhu[3], Naoki Kimura[1], Motohiro Okada[4], Masaki Nishimura[5], Nobuyuki Kimura[6], Shigeo Murayama[7,8], Sunao Kaneko[9], Ryuichi Shigemoto[10], Keiji Imoto[11] and Toshiharu Suzuki[1*]

Abstract

Background: One of the best-characterized causative factors of Alzheimer's disease (AD) is the generation of amyloid-β peptide (Aβ). AD subjects are at high risk of epileptic seizures accompanied by aberrant neuronal excitability, which in itself enhances Aβ generation. However, the molecular linkage between epileptic seizures and Aβ generation in AD remains unclear.

Results: X11 and X11-like (X11L) gene knockout mice suffered from epileptic seizures, along with a malfunction of hyperpolarization-activated cyclic nucleotide gated (HCN) channels. Genetic ablation of HCN1 in mice and HCN1 channel blockage in cultured Neuro2a (N2a) cells enhanced Aβ generation. Interestingly, HCN1 levels dramatically decreased in the temporal lobe of cynomolgus monkeys (*Macaca fascicularis*) during aging and were significantly diminished in the temporal lobe of sporadic AD patients.

Conclusion: Because HCN1 associates with amyloid-β precursor protein (APP) and X11/X11L in the brain, genetic deficiency of X11/X11L may induce aberrant HCN1 distribution along with epilepsy. Moreover, the reduction in HCN1 levels in aged primates may contribute to augmented Aβ generation. Taken together, HCN1 is proposed to play an important role in the molecular linkage between epileptic seizures and Aβ generation, and in the aggravation of sporadic AD.

Background

Alzheimer's disease (AD) is characterized by progressive memory impairment, which accompanies aging. Genetic and biochemical studies show that the production of amyloid-β peptide (Aβ) largely contributes to the etiology of AD [1]. Aβ is generated from amyloid-β precursor protein (APP) by β- and γ-cleavage of the latter.

The risk of seizure activity is particularly high in AD patients, with an 87-fold increase in subjects with early-onset dementia compared with an age-matched reference population [2-7]. Factors linking seizure activity to Aβ generation in AD patients remain unclear, although epilepsy is believed to result from abnormal regulation of neuronal excitability, which favors hypersynchrony. In addition, increased neuronal activity enhances Aβ production from APP [8-10].

Hyperpolarization-activated cyclic nucleotide gated HCN channels 1–4 (HCN1–4) conduct inward, depolarizing mixed Na^+/K^+ currents and thereby control resting membrane potential, dendritic integration, synaptic transmission, and rhythmic activity in cardiac pacemaker cells and spontaneous firing neurons [11]. Dysregulation of these channels and their hyperpolarization-activated (Ih) currents is strongly implicated in various experimental animal models of epilepsy, as well as in human epilepsy patients [12]. Furthermore, HCN2 co-assembles with the X11-like (X11L) protein [13], which is a metabolic regulator of APP processing [14].

X11 proteins (X11s) comprise a family of three evolutionarily conserved molecules (X11/X11α/Mint1, X11L/

* Correspondence: tsuzuki@pharm.hokudai.ac.jp
[1]Laboratory of Neuroscience, Graduate School of Pharmaceutical Sciences, Hokkaido University, Kita12-Nishi6, Kita-ku, Sapporo 060-0812, Japan
Full list of author information is available at the end of the article

X11β/Mint2, and X11L2/X11γ/Mint3). These proteins bind to the cytoplasmic region of APP in cultured cells and suppress its metabolism [15,16]. Moreover, the metabolism of overexpressed human APP (hAPP) is suppressed in X11 and X11L transgenic mice, along with the generation of Aβ [17-19]. On the other hand, mutant mice lacking X11L ($X11^{+/+}/X11L^{-/-}$ mice) or both X11 and X11L ($X11^{-/-}/X11L^{-/-}$ mice) facilitate amyloidogenic metabolism of endogenous murine APP and exogenous hAPP, including Aβ generation [20-22]. Therefore, inactivation of X11/X11L clearly increases the production of Aβ, potentially contributing to the pathology of AD.

Here, we report that i) $X11^{-/-}/X11L^{-/-}$ mice suffer from spontaneous epileptic seizures along with malfunction of HCN channel activity; ii) HCN1 can form a complex with APP and X11 or X11L in the murine brain; iii) $HCN1^{-/-}$ gene knockout mice show enhanced Aβ generation; iv) overexpression of HCN1 in Neuro2a (N2a) cells decreases Aβ generation, whereas blockage of HCN1 channel activity in N2a cells restores the level of Aβ production; v) the level of HCN1 diminishes significantly in the temporal cortex of cynomolgus monkeys (*Macaca fascicularis*) during aging; and vi) HCN1 levels are significantly reduced in the brains of sporadic AD patients compared with the brains of age-matched healthy subjects.

Given the previous reports and our current observations, we hypothesize that X11 and X11L play an important role in the modulation of HCN channel function, the dysregulation of which correlates with epilepsy. We further hypothesize that the impairment of HCN channels, and in particular HCN1, accompanies with the aberrant production of Aβ, which manifests as neurotoxicity. Thus, HCN1 together with X11 and X11L may provide a molecular link between seizure activity and Aβ generation in AD patients.

Results

Spontaneous epileptic seizures caused by X11 and X11L gene deficiency

Electrocorticograms were recorded in $X11^{+/+}/X11L^{+/+}$ (wild type), $X11^{+/+}/X11L^{-/-}$, $X11^{-/-}/X11L^{+/+}$, and $X11^{-/-}/X11L^{-/-}$ mice. We found that $X11^{-/-}/X11L^{-/-}$ mice suffered from spontaneous epileptic seizures at the age of 13 weeks and over (detailed results are provided in Additional file 1: Figure S1 and Additional file 2: Movies S1, Additional file 3: Movies S2 and Additional file 4: Movies S3). Three out of four $X11^{-/-}/X11L^{-/-}$ mice showed an abnormal electrocorticogram recording within 48 h, namely, the presence of epileptic discharge, which were never observed in $X11^{+/+}/X11L^{+/+}$, $X11^{+/+}/X11L^{-/-}$, or $X11^{-/-}/X11L^{+/+}$

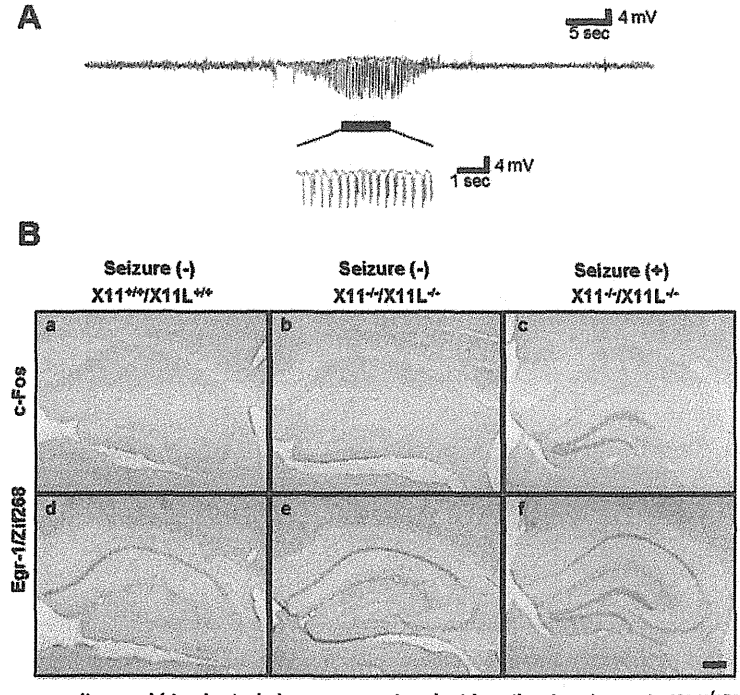

Figure 1 Electrocorticogram recording and histological changes associated with epileptic seizures in $X11^{-/-}/X11L^{-/-}$ mice. (*A*) An electrocorticogram recorded in 13-week-old $X11^{-/-}/X11L^{-/-}$ mice (n = 4). Epileptic discharges are underlined. (*B*) c-Fos (*a, b, c*) and Egr-1/zif268 (*d, e, f*) immunoreactivity in the hippocampus of $X11^{+/+}/X11L^{+/+}$ (*a, d*) and $X11^{-/-}/X11L^{-/-}$ (*b, c, e, f*) mice under steady-state conditions (*a, b, d, e*) and at 90 min after an epileptic episode (*c, f*). Scale bar, 200 μm.

mice (Figure 1, Additional file 1: Figure S1 and Additional file 4: Movie S3). Subsets of $X11^{-/-}/X11L^{-/-}$ mice went into status epilepticus and died.

Seizures are often associated with the augmented expression of immediate-early genes in neurons [23]. We first asked whether such gene activation was observed in $X11^{-/-}/X11L^{-/-}$ mice following epileptic seizures and investigated the involvement of specific brain regions in seizure activity. Brain tissue sections from $X11^{-/-}/X11L^{-/-}$ mice were immunostained for c-Fos, a calcium-dependent immediate-early gene product, and Egr-1/Zif268, an early growth response transcription factor, within 90 min of a seizure event. The brains of these mice showed enhanced expression of both c-Fos and Egr-1/Zif268 in the dentate gyrus (DG) granule cells compared with the brains of $X11^{+/+}/X11L^{+/+}$ and $X11^{-/-}/X11L^{-/-}$ mice (Figure 1B). However, we cannot rule out a possibility that subclinical discharges without aberrant behavior may

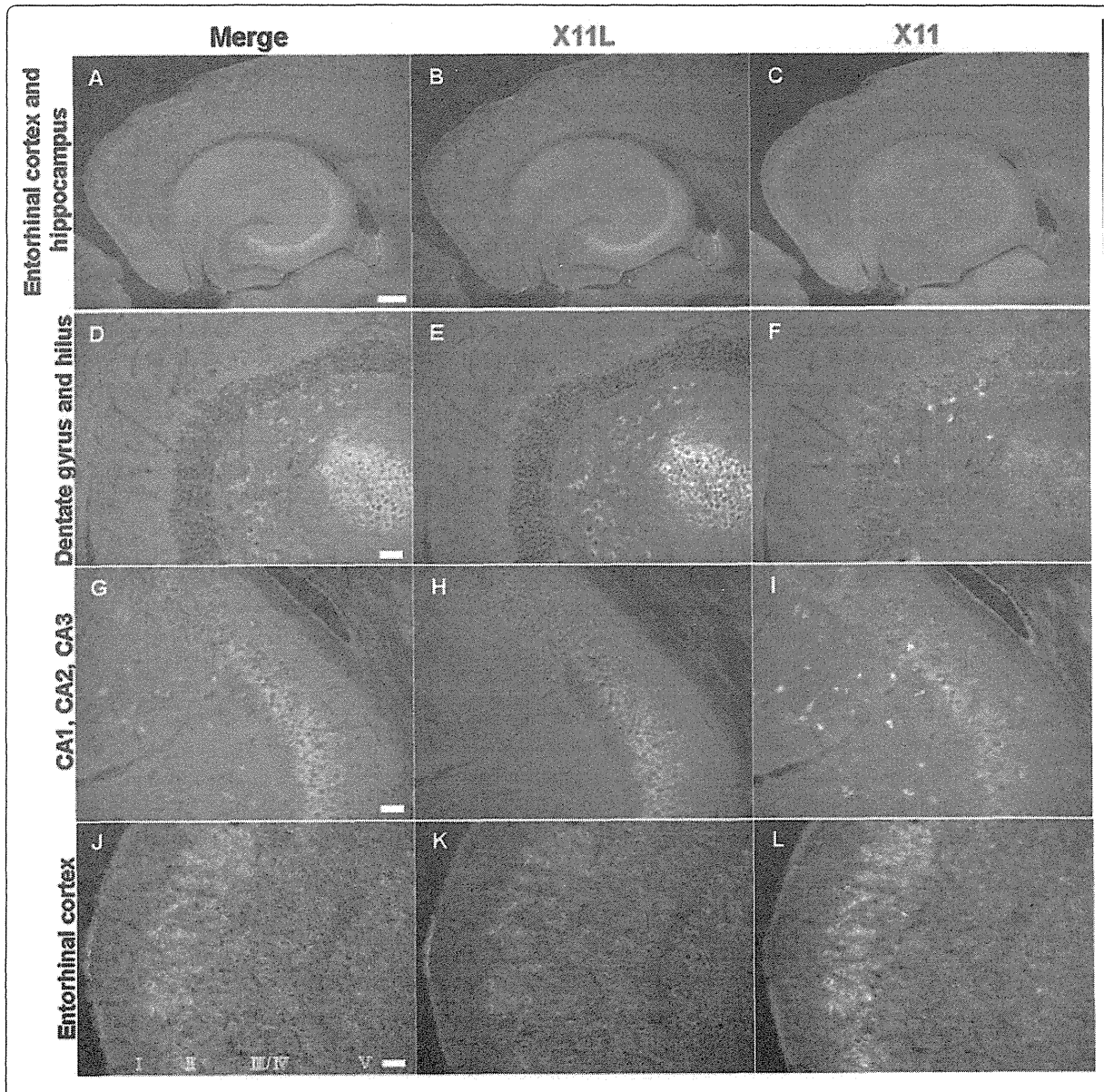

Figure 2 Expression of X11 and X11L in the 13-week-old mouse brain. Representative images of horizontal brain sections from 13-week-old $X11^{+/+}/X11L^{+/+}$ mice were stained for X11 (***C, F, I, L***) and X11L (***B, E, H, K***). Immunohistochemistry was performed with anti-X11 polyclonal rabbit IgG followed by donkey anti-mouse IgG conjugated to Alexa Fluor 488, and anti-X11L monoclonal mouse IgG followed by donkey anti-rabbit IgG conjugated to Cy3. Merged images are shown in the *left panels* (***A, D, G, J***). Blue signals indicate nuclei counter-stained with DAPI. Scale bars, 300 μm (***A–C***), 50 μm (***D–L***).

cause the enhanced expression of c-Fos and Egr-1/Zif268. Thus, a deficiency in both X11 and X11L may cause abnormal, seizure-associated neuronal activity and subsequent alterations in protein expression in the hippocampal formation.

Reduction of Ih currents in entorhinal cortex (EC) layer II of $X11^{-/-}/X11L^{-/-}$ mice

Spontaneous epileptic seizures were observed in mice when both X11 and X11L genes were deficient (Figure 1A, Additional file 1: Figure S1 and additional movies). Because the DG granule cells of $X11^{-/-}/X11L^{-/-}$ mice showed augmented expression of c-Fos and Egr-1/Zif268 following seizure activity, we next performed a detailed examination of the expression of both proteins in hippocampal neurons in 13-week-old murine brains (Figure 2).

Distinct expression patterns of X11 and X11L were observed in the hippocampus of wild type mice. X11L was expressed mainly in the pyramidal neurons of the CA1–3 region (Figure 2B, E, H), whereas X11 was expressed in other types of interneurons (Figure 2C, F, I). These observations coincide with our previous report of X11s expression in aged wild type mice [21]. Unlike c-Fos and Egr-1/Zif268 in the double mutant mouse, X11 and X11L were not expressed in DG granule cells (Figure 2D–F). However, both X11 and X11L were strongly co-expressed in EC layer II (Figure 2J–L), which projects axons primarily to the granule cells of the DG [24]. Furthermore, both HCN1 and HCN2 are expressed in EC layer II [25]. Given that $HCN1^{-/-}$ mice show enhanced seizure susceptibility and that $HCN2^{-/-}$ mice suffer from absence seizures [26,27], we next focused our investigations on the alteration of Ih currents associated with HCN channels in EC layer II in $X11^{-/-}/X11L^{-/-}$ mice.

Horizontal brain slices that included the EC and the hippocampus were prepared from 12–14-week-old $X11^{+/+}/X11L^{+/+}$, $X11^{+/+}/X11L^{-/-}$, $X11^{-/-}/X11L^{+/+}$, and $X11^{-/-}/X11L^{-/-}$ mice. EC layer II neurons were then subjected to electrophysiological analysis, and Ih currents from HCN channels were recorded (Figure 3 and Additional file 1: Figure S2). The mice used in the electrophysiological study were seizure-naïve, at least without over behavioral manifestations, and showed comparable levels of HCN1 channels in the EC (Additional file 1: Figure S3). Similar to a previous report [28], hyperpolarizing voltage steps activated a large Ih current in EC layer II cells of $X11^{+/+}/X11L^{+/+}$ mice (Figure 3A and C). By contrast, the Ih current was dramatically reduced in $X11^{-/-}/X11L^{-/-}$ mice relative to that in $X11^{+/+}/X11L^{+/+}$ mice (Figure 3B and D); however, no significant alterations were observed for the V1/2 (mean ± SEM, $X11^{+/+}/X11L^{+/+}$: −81.1±1.1 mV; $X11^{-/-}/X11L^{+/+}$: −80.3±1.3 mV; $X11^{+/+}/X11L^{-/-}$: −83.5±1.4 mV; $X11^{-/-}/X11L^{-/-}$: −81.3±0.9 mV) (Figure 3E) or the series resistance (mean ± SEM, $X11^{+/+}/X11L^{+/+}$: 8.3±0.2 MΩ; $X11^{-/-}/X11L^{+/+}$: 8.9±0.5 MΩ; $X11^{+/+}/X11L^{-/-}$: 9.2±0.4 MΩ; $X11^{-/-}/X11L^{-/-}$: 8.0±0.2 MΩ) (Figure 3F). Quantitative analysis (Figure 3G) revealed that the density of the Ih current was also significantly reduced in $X11^{-/-}/X11L^{-/-}$ mice (1.12±0.15 pA/pF, n = 9; $p < 0.01$) compared with that in $X11^{+/+}/X11L^{+/+}$ mice (2.18±0.27 pA/pF, n = 10), but did not change significantly in $X11^{-/-}/X11L^{+/+}$ mice (2.41±0.25 pA/pF, n = 9, $p > 0.05$) or in $X11^{+/+}/X11L^{-/-}$ mice (2.05±0.29 pA/pF, n = 9, $p > 0.05$). Thus, genetic ablation of X11 and X11L together had a profound impact on the Ih current in the EC layer II of the double knockout mice. These results correlate with the observation that $X11^{-/-}/X11L^{-/-}$ mice, but not $X11^{+/+}/X11L^{+/+}$, $X11^{+/+}/X11L^{-/-}$, or $X11^{-/-}/X11L^{+/+}$ mice, are susceptible to spontaneous epileptic seizures.

In EC layer II, the dominant HCN subtype is HCN1 [28]. We found that HCN1, X11, and X11L were colocalized in EC layer II neurons (Figure 3H) and apparently formed a complex in the brain (Figure 3I–K). The colocalization of these molecules was observed in a region surrounding the neuronal nucleus (Figure 3H), consistent with the location of the Golgi apparatus. Because X11 and X11L are largely localized in the Golgi apparatus and function in the trafficking of membrane proteins [29,30], the deletion of X11 and X11L may disturb intracellular localization of HCN channels (Additional file 1: Figure S4). While the localization of the channel likely affects its function, we cannot rule out the possibility that X11 and X11L directly regulate HCN1 function as well.

Enhanced Aβ generation according to HCN1 dysfunction

The EC is one of the most vulnerable brain regions in AD [31], and it is well-known that synaptic activity such as that mediated by HCN channels can regulate Aβ generation [8-10]. Therefore, we examined whether HCN channel impairment involved in the aberrant production of Aβ. We first quantified the levels of endogenous Aβ40 and Aβ42 in $HCN1^{-/-}$ mouse brains. Aβ40 and Aβ42 were both significantly increased in the cortex of $HCN1^{-/-}$ mice compared with $HCN1^{+/+}$ mice (average ± SEM, Aβ40: n = 5, $p = 0.0037$; Aβ42: n = 5, $p = 0.0055$) (Figure 4A). The magnitude of the increase in Aβ40 and Aβ42 was inversely proportional to the level of HCN1 gene expression (Figure 4A, left panel), while APP protein levels were comparable in $HCN1^{+/+}$, $HCN1^{+/-}$, and $HCN1^{-/-}$ mice (Figure 4A, right panel).

To confirm whether the increase in Aβ generation in $HCN1^{-/-}$ mice depends on the decrease in HCN channel activity, we used N2a cells that transiently overexpressed FLAG-APP and HCN1 (Figure 4B). Overexpression of HCN1 significantly reduced the generation of Aβ40 and Aβ42 (compare column 2 with column 3 for each Aβ peptide). The Aβ levels were restored by adding ZD7288, a

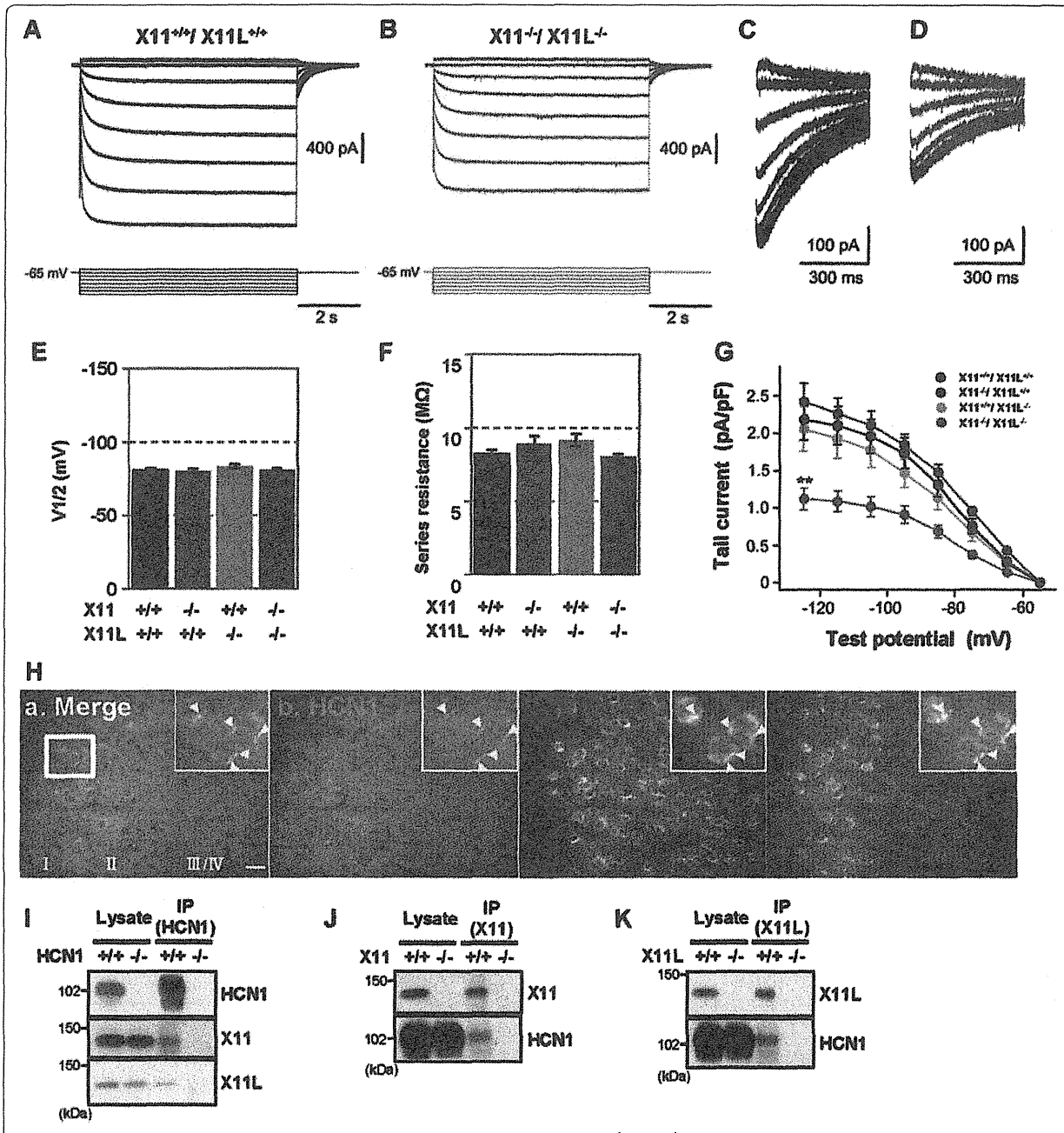

Figure 3 Reduction of Ih currents in entorhinal cortex layer II neurons of $X11^{-/-}/X11L^{-/-}$ mice. (***A, B***) Representative electrophysiological recordings of Ih currents from EC layer II neurons in $X11^{+/+}/X11L^{+/+}$ (***A***) and $X11^{-/-}/X11L^{-/-}$ (***B***) mice. (***C, D***) Tail currents of $X11^{+/+}/X11L^{+/+}$ (***C***) and $X11^{-/-}/X11L^{-/-}$ (***D***) mice. (***E***) Quantitative data of the voltage, whereby the current is half-activated (V1/2). Statistical analysis was performed using one-way analysis of variance followed by Tukey's multiple comparison test (mean ± SEM (mV); five slices from two $X11^{+/+}/X11L^{+/+}$ mice, n = 10; four slices from two $X11^{-/-}/X11L^{+/+}$, $X11^{+/+}/X11L^{-/-}$, and $X11^{-/-}/X11L^{-/-}$ mice, n = 9). (***F***) Quantitative data of series resistance. Statistical analysis was performed as described (mean ± SEM (MΩ); five slices from two $X11^{+/+}/X11L^{+/+}$ mice, n = 10; four slices from two $X11^{-/-}/X11L^{+/+}$, $X11^{+/+}/X11L^{-/-}$, and $X11^{-/-}/X11L^{-/-}$ mice, n = 9). (***G***) Summary of the current density of the tail currents. Statistical analysis was performed as described (mean ± SEM (pA/pF); five slices from two $X11^{+/+}/X11L^{+/+}$ mice, n = 10; four slices from two $X11^{-/-}/X11L^{+/+}$, $X11^{+/+}/X11L^{-/-}$, and $X11^{-/-}/X11L^{-/-}$ mice, n = 9; $^{**}p < 0.01$). (***H***) Representative images of the HCN1-X11-X11L complex in EC layer II neurons of 13-week-old $X11^{+/+}/X11L^{+/+}$ mice (a, merge; b HCN1 (green); c, X11L (red); d, X11(blue)). Scale bar, 20 μm. (***I–K***) Co-immunoprecipitation of HCN1-X11s complexes from the 13-week-old $X11^{+/+}/X11L^{+/+}$ murine cortex. $HCN1^{-/-}$ (***I***), $X11^{-/-}$ (***J***), or $X11L^{-/-}$ (***K***) mice were used as controls. Brain lysates were immunoprecipitated with anti-HCN1 (***I***), anti-X11 (***J***), and anti-X11L/Mint2 (***K***) antibodies. Immunocomplexes were detected by immunoblotting.

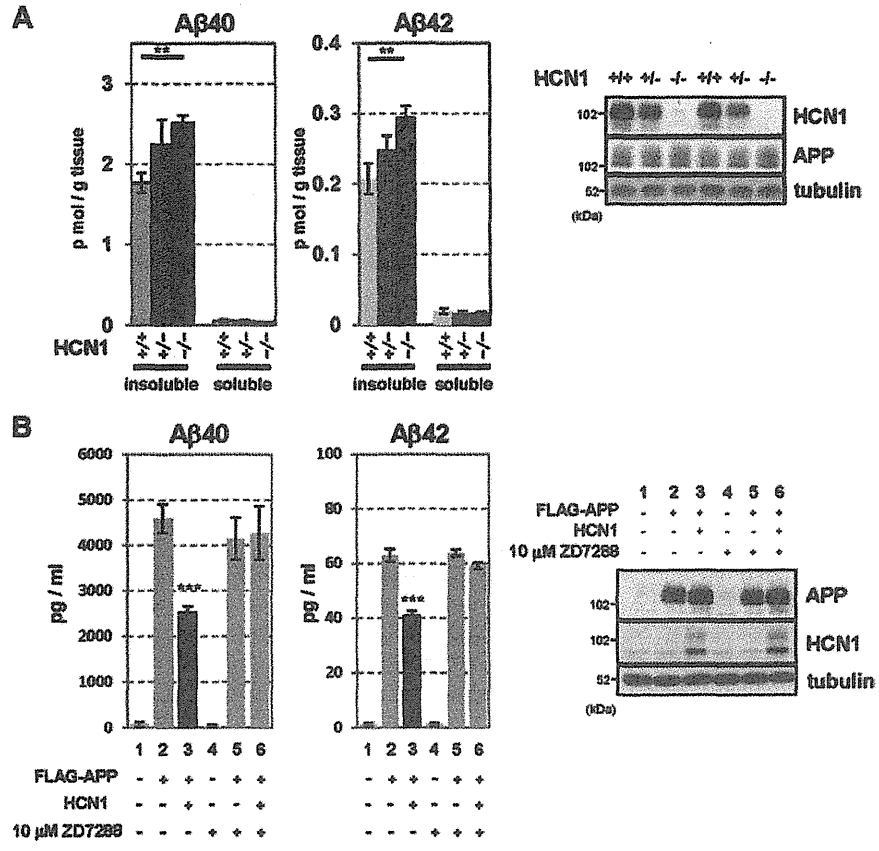

Figure 4 Functional deficits in the HCN1 channel facilitate Aβ generation. (*A*) Quantification of endogenous murine Aβ40 and Aβ42 in the cortex of 4-month-old $HCN1^{+/+}$, $HCN1^{+/-}$, and $HCN1^{-/-}$ mice by using the sELISA system (left panels). Statistical analysis was performed using the two-tailed Mann–Whitney *U*-test (average ± SEM, n = 5, **p < 0.01). (*B*) Quantification of Aβ40 and Aβ42 secreted into the culture medium by N2a cells by using the sELISA system. FLAG-APP or FLAG-APP and HCN1 were transiently overexpressed in the cells with (+) or without (–) 10 μM ZD7288 (left panels). Statistical analysis was performed using one-way analysis of variance followed by Tukey's multiple comparison test (average ± SEM, n = 4, ***p < 0.001). Expression levels of APP and HCN1 was confirmed by immunoblotting (right panels in *A* and *B*).

selective inhibitor of HCN channel activity (compare lanes 3 through 6). Although we have not confirmed the blockage of channel activity electrophysiologically, ZD7288 had no effect on Aβ levels in cells without HCN1 expression (column 5), and APP expression was not affected by either the presence of HCN1 or by the administration of ZD7288 (Figure 4B, right panel). Furthermore, administration of ZD7288 did not influence the interaction of HCN1 with APP (Additional file 1: Figure S5). These results suggest that the suppression of Aβ generation in HCN1-overexpressing cells probably depends on channel activity (Figure 4B), in agreement with the *in vivo* observation that the brains of mice lacking the HCN1 gene and with impaired HCN channel activity (Figure 3B, D, and G) demonstrated increased Aβ generation (Figure 4A).

Association of HCN1 with APP *in vivo* and *in vitro*

Increased synaptic activity enhances Aβ generation [8-10], and modulation of Aβ generation is not limited to alterations in HCN1 channel activity. Indeed, APP metabolism is thought to be largely regulated by APP-binding partners [14]. Therefore, we next explored the hypothesis that HCN1 might be involved in regulating APP metabolism via a physical interaction between the channel and APP. In support of this hypothesis, an anti-HCN1 antibody co-immunoprecipitated APP together with HCN1 from a lysate of wild type murine cortex (Figure 5A). The interaction seemed to be specific in that APP was not recovered from the cortical lysate of $HCN1^{-/-}$ mice. The association between APP and HCN1 was next confirmed in the EC. Using EC-rich brain samples isolated from $HCN1^{+/+}$ and $HCN1^{-/-}$ mice (Additional file 1: Figure S3A), a co-immunoprecipitation assay was performed with an anti-HCN1 antibody, and the immunoprecipitates were analyzed with the indicated antibodies (Figure 5B). Along with X11 and X11L, APP was co-immunoprecipitated with HCN1 in EC-rich brain samples of wild type mice (Figure 5B), suggesting that HCN1 can complex with

APP and X11/X11L *in vivo*. These results are in agreement with the co-localization results of HCN1, X11, and X11L in the wild type cortex shown above (Figure 3H–K). Tubulin and PSD95 (postsynaptic density protein 95) were not detected in the immunocomplex, indicating the specific association of APP and X11/X11L with HCN1.

To show whether HCN1 directly binds to APP without mediation by X11/X11L, FLAG-APP and HCN1 were transiently expressed in N2a cells and a co-immunoprecipitation

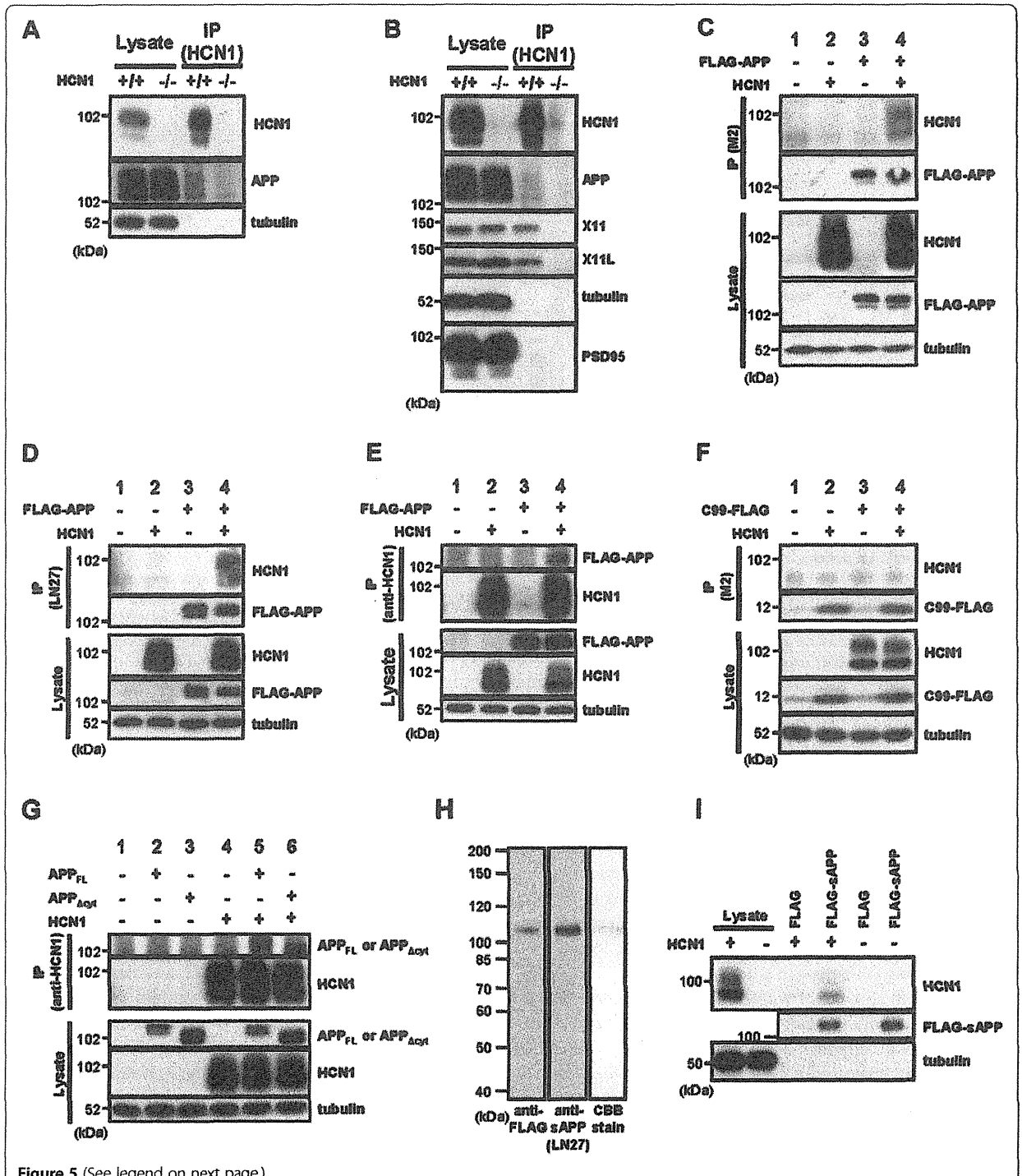

Figure 5 (See legend on next page.)

(See figure on previous page.)
Figure 5 APP and HCN1 form a molecular complex *in vivo* and *in vitro*. (***A***) Co-immunoprecipitation of the HCN1-APP complex from the wild type and HCN1$^{-/-}$murine cortex. Brain lysates were immunoprecipitated with an anti-HCN1 antibody. Immunocomplexes were detected by immunoblotting. (***B***) Co-immunoprecipitation of HCN1-APP, -X11 and -X11L complexes from the EC-rich cortex (see Additional file 1: Figure S2). Brain lysates were immunoprecipitated with an anti-HCN1 antibody. Immunocomplexes were detected by immunoblotting. (***C–G***) Co-immunoprecipitation of the HCN1-APP complex from N2a cells transiently overexpressing FLAG-APP and murine HCN1. (***C–E***), Analysis of FLAG-APP and murine HCN1, (***F***) C99-FLAG and murine HCN1, and (***G***) APP_{FL} or $APP_{\Delta cyt}$ and murine HCN1 immunocomplexes. To standardize the amount of plasmid, empty vector (–) was added to yield 1.2 μg of plasmid in total. Cell lysates were immunoprecipitated with anti-FLAG M2 (*C* and *F*), anti-APP extracellular domain (LN27) (*D*), or anti-HCN1 (***E*** and ***G***) antibodies. Immunocomplexes were detected by immunoblotting. (***H***) Affinity purification of FLAG-sAPP secreted into the culture medium by N2a cells expressing FLAG-APP. The purification was performed using anti-FLAG M2 affinity beads. FLAG-sAPP were specifically detected by M2 and anti-APP extracellular domain (LN27) antibodies, and no contaminating bands were identified by CBB-staining. (***I***) Pull-down of HCN1 with affinity purified FLAG-sAPP prepared in (H). Lysates from wild type cells (–) and cells that transiently expressed HCN1 (+) were incubated with M2 affinity beads coupled with FLAG-tag or FLAG-sAPP. The complexes resulting from the pull-down assay were subjected to immunoblot analysis with anti-HCN1 antibody.

assay was performed. The anti-FLAG M2 antibody immunoprecipitated HCN1 along with FLAG-APP (Figure 5C). An anti-hAPP extracellular domain antibody (LN27) also recovered HCN1 (Figure 5D), and anti-HCN1 antibody recovered FLAG-APP (Figure 5E).

APP is a type I transmembrane protein composed of a large extracellular (luminal) domain of 596 amino acids and a small intracellular domain of 47 amino acids. On the other hand, HCN1 is six-transmembrane protein with short extracellular sequences between transmembrane regions one and two, three and four, and five and six; and long intracellular domains within the amino- and carboxyl-terminal regions of the protein. To determine the region of APP that binds to HCN1, we performed co-immunoprecipitation assays using APP deletion mutants (C99-FLAG, which largely lacks the extracellular domain of APP and in which FLAG is fused to the carboxyl terminal region of APP; and $APP_{\Delta cyt}$, which lacks the 43- amino acid carboxyl terminal region of APP) (Figure 5F, G). The results of this assay indicated that HCN1 was not co-immunoprecipitated with C99-FLAG (Figure 5F), whereas $APP_{\Delta cyt}$ was co-immunoprecipitated with HCN1 (Figure 5G).

Next, we performed an *in vitro* pull-down assay with FLAG-soluble APP (FLAG-sAPP, consisting of the extracellular domain of APP cleaved at the α- and/or β-cleavage sites). FLAG-sAPP was purified with affinity beads (anti-FLAG M2 affinity gel) from the culture medium of N2a cells expressing FLAG-APP (Figure 5H) and then incubated with lysates of N2a cells that expressed HCN1. HCN1 bound to FLAG-sAPP, but not to FLAG-tag alone (Figure 5I). Taken together, the results shown in Figure 5 indicate that HCN1 associates with APP through its extracellular (luminal) domain.

Hence, HCN1 apparently interacts with the extracellular domain of APP (Figure 5) and with both X11 and X11L in the cytoplasm (Figure 3H–K, Figure 5B). This suggests that the HCN1 channel might form a ternary complex with APP and either X11 or X11L to regulate Aβ generation. However, the detailed molecular regulation of complex formation remains to be determined.

Age- and AD state-dependent HCN disruption in the temporal cortex (superior temporal gyrus) of cynomolgus monkeys and sporadic AD patients

Advanced age is the greatest risk factor for AD. To examine the relationship between aging and HCN1 levels, we quantified the amount of HCN1, Aβ, APP, and actin in freshly frozen brain tissues (superior temporal gyrus) from cynomolgus monkeys of various ages (Figure 6A and Additional file 1: Figure S6). Senile plaques and neurofibrillary tangles spontaneously appear in the brains of cynomolgus monkeys with advancing age [32,33], and the amino acid sequence of Aβ in cynomolgus monkeys is identical to that in humans [34]. Thus, we hypothesized that the cynomolgus monkey would be a useful animal model for the investigating the relationship between aging and AD pathology. Significant negative correlations were found between HCN1 levels and age ($n = 39$, $r = -0.5363$, $p = 0.0004$) (Figure 6A, left), between HCN1 and APP levels ($n = 39$, $r = -0.3796$, $p = 0.0086$) (Additional file 1: Figure S6B), between HCN1 and TBS-insoluble Aβ40 levels ($n = 39$, $r = -0.2878$, $p = 0.0421$) (Additional file 1: Figure S6C and D), and between HCN1 and Tris buffered saline (TBS)-insoluble Aβ42 levels ($n = 39$, $r = -0.2913$, $p = 0.0401$) (Additional file 1: Figure S6E and F). A significant positive correlation was found between age and APP level ($n = 39$, $r = 0.8156$, $p < 0.0001$) (Additional file 1: Figure S6A), and a significant weak-positive correlation was found between APP and TBS-insoluble Aβ42 levels ($n = 39$, $r = 0.3714$, $p = 0.0236$) (Additional file 1: Figure S6H). However, no correlation was found between age and actin level ($n = 39$, $r = -0.1981$, $p = 0.2266$) (Figure 6A, right) or between APP and TBS-insoluble Aβ40 levels ($n = 39$, $r = 0.2993$, $p = 0.072$) (Additional file 1: Figure S6G).

Finally, we examined the possibility of altered HCN1 levels in human AD brain specimens obtained at autopsy

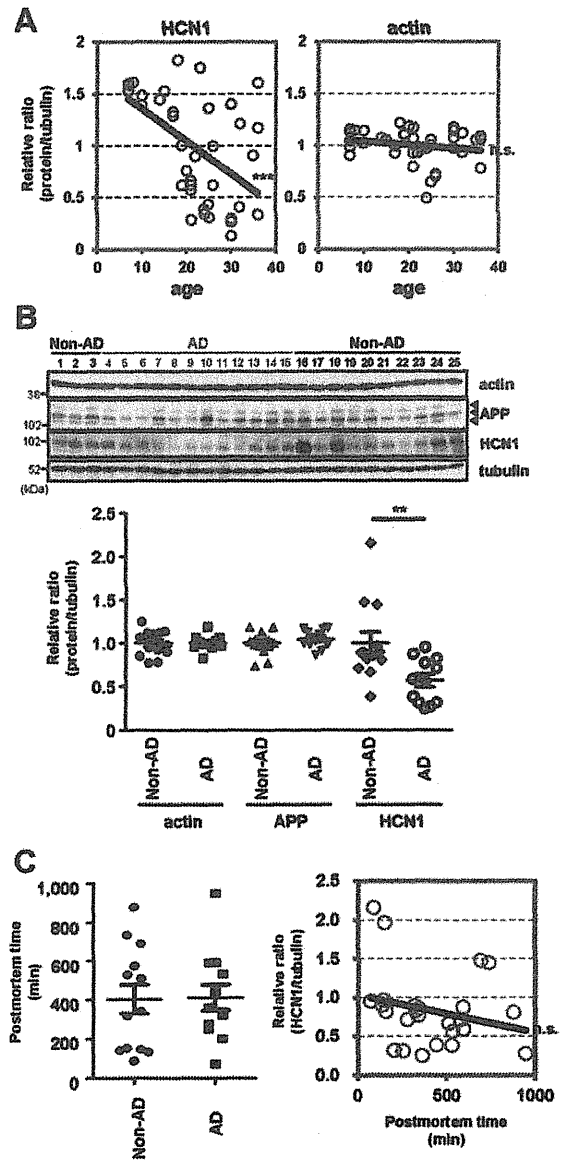

Figure 6 HCN1 levels decrease in a age- and AD-dependent manner. (*A*) Quantification of the amount of HCN1 and actin in the brain (superior temporal gyrus) of 4–37-year-old cynomolgus monkeys by immunoblotting. Statistical analysis was performed using the two-tailed Pearson's correlation coefficient (HCN1: n = 39, r = −0.5363, ***p < 0.001; actin: n = 39, r = −0.1981, p > 0.05). (*B*) Quantification of the amount of HCN1, APP, actin, and tubulin in age-matched AD and non-AD postmortem brains (superior temporal gyrus) by immunoblotting. Statistical analysis was performed using the two-tailed Mann–Whitney *U*-test (non-AD: n = 13, AD: n = 12, **p < 0.01). (*C*) Comparison of postmortem time between non-AD and AD samples. Statistical analysis was performed using the two-tailed Mann–Whitney *U*-test (non-AD: n = 13, AD: n = 12, p = 0.8066). The correlation between postmortem time and HCN1 level was analyzed. Statistical analysis was performed using the two-tailed Pearson's correlation coefficient (n = 39, r = −0.2416, p = 0.2446). Descriptions of all subjects are provided in Table 1.

(Figure 6B and Table 1). The postmortem time was not significantly different for the AD and non-AD brain samples used in this study (non-AD: n = 13, AD: n = 12, $p = 0.8066$), and no significant decrease in HCN1 levels related to postmortem time was observed (n = 25, r = −0.2416, $p = 0.2446$) (Figure 6C and Table 1). Of great relevance to this study, the amount of HCN1 was significantly reduced in AD brains (superior temporal gyrus) compared with that in age-matched control brains (non-AD: n = 13, AD: n = 12, $p = 0.0083$), while the levels of APP and actin were not significantly altered (Figure 6B and Table 1). These results suggest that the reduction in HCN1 expression that occurs with age (Figure 6A) may be involved in the aggravation of the pathology of AD.

Discussion

X11 and X11L are well-characterized neural adaptor proteins that regulate the trafficking and metabolism of APP [14]. Many reports indicate that X11s bind to APP and suppress Aβ generation *in vitro* and *in vivo* [14-22]. Furthermore, X11s are thought to mediate a number of cellular functions through their association with various proteins [35]. This report showed that mutant mice lacking both X11 and X11L present with dysfunctional HCN1 channel activity and epileptic seizures. Notably, AD patients are also at increased risk of epileptic seizures. Furthermore, mutant mice lacking HCN1 demonstrated increased generation of Aβ, which is a causative factor for the development of AD.

The incidence of AD dramatically increases with age. We found that the amount of HCN1 decreased with both aging and in AD. The dysfunction of HCN1 that occurs over time may, thus, be a trigger for epileptic seizures and the pathogenic generation of Aβ in AD.

Several converging studies corroborate the premise that HCN channel activity is closely related to epileptogenesis [11]. For example, HCN1 expression is significantly reduced in the EC after temporal lobe epilepsy [36,37]. Furthermore, HCN1 channel plasticity in cortical neurons is similar in multiple epileptic animal models [38-43]. Moreover, kainic acid-induced seizure susceptibility is increased in $HCN1^{-/-}$ mice [27], and HCN2-deficient mice exhibit spontaneous absence seizures [26].

$HCN1^{-/-}$ mice show a significantly higher number of negative resting membrane potentials and a significantly higher input resistance measured from responses to either negative or positive current steps [28]. As such, seizure susceptibility is increased in $HCN1^{-/-}$ mice [27], indicating that loss of the HCN1 subunit enhances neuronal excitability, which can increase Aβ generation [8-10]. These observations suggest that enhanced Aβ generation in $HCN1^{-/-}$ mice results from neuronal hyper-excitability, which is in turn caused by ablation of the HCN1 gene.

Table 1 Summary of subject information presented in Figure 6B and C

Sample no.	Subject	Age	Sex	Post mortem time (min)	Braak stage	Seizure	Relative ratio (protein/tubulin)		
							Actin	APP	HCN1
1	Normal	84	F	877	1	-	0.929	1.192	0.809
2	Normal	88	F	144	1	-	0.856	1.046	0.859
3	Normal	70	M	340	0.5	-	0.955	1.189	0.859
4	AD	84	M	71	4	-	0.950	1.171	0.952
5	AD	70	M	276	4	-	0.829	0.986	0.716
6	AD	74	M	322	5	-	0.961	0.990	0.827
7	AD	75	M	594	6	-	1.069	1.176	0.589
8	AD	76	M	947	6	+	1.190	1.167	0.273
9	AD	79	F	203	5	-	1.019	0.913	0.317
10	AD	81	M	360	6	-	0.971	0.862	0.247
11	AD	81	F	442	5	-	0.971	0.862	0.385
12	AD	82	F	254	6	-	0.988	1.029	0.313
13	AD	82	F	533	5	-	0.988	1.001	0.566
14	AD	82	F	338	4	-	1.028	1.063	0.770
15	AD	84	M	590	5	-	1.071	1.128	0.876
16	Normal	78	F	87	2	-	1.108	1.138	2.153
17	Normal	81	M	134	1	-	1.122	0.971	0.902
18	Normal	82	F	148	1	-	1.178	1.109	1.963
19	Normal	82	F	155	2	-	1.141	1.026	0.821
20	Normal	80	M	317	2	-	1.254	1.037	0.893
21	Normal	80	M	510	2	-	1.071	0.778	0.669
22	Normal	82	M	530	1	-	0.979	0.916	0.384
23	Normal	78	M	575	1	-	0.905	1.007	0.713
24	Normal	78	M	690	1	-	0.784	0.986	1.479
25	Normal	82	M	736	1	-	0.774	0.743	1.448

Postmortem brain samples were obtained from the Brain Bank for Aging Research, Tokyo Metropolitan Institute of Gerontology. Experimental procedures were approved by the appropriate ethical boards at each institute. Autopsies were performed with written informed consent from the patients or their relatives. The clinical diagnosis of AD was based on two major criteria: the Diagnostic and Statistical Manual of Mental Disorders: 4th Edition (DSM-IV) and the National Institute of Neurological and Communicational Disorders and Stroke-Alzheimer's Disease and Related Disorders Association (NINCDS-ADRDA). The neuropathological diagnosis of AD was made using Consortium to Establish a Registry for Alzheimer's Disease criteria (average age at death, 79.2 ± 4.4 years). Control brains were obtained from age-matched individuals with no history of neurological or psychiatric illness (average age at death, 80.4 ± 4.2 years). Subjects, age, gender, postmortem time, Braak stage, seizure history, and relative protein/tubulin ratios are indicated.

On the other hand, the present study showed that HCN1 physically associated with APP through the extracellular domain of APP. Therefore, HCN1-mediated regulation of Aβ generation may depend on a molecular linkage between HCN1 and APP and not simply on alterations in neuronal excitability. However, the molecular mechanism by which HCN1 potentially links epileptic seizures to Aβ generation in AD remains to be elucidated.

Our results suggest that ablation of X11/X11L induces aberrant HCN1 distribution and function along with epilepsy. Although the molecular mechanism by which X11s regulates HCN channel activity also remains unclear, X11s are known to modulate intracellular trafficking of membrane proteins. For example, X11s interact with certain proteins implicated in traffic and transport, such as Arfs, Rab6, and KIF17 [29,44,45]. Furthermore, X11s bind to vesicular cargo proteins, such as APP and alcadein [16,46,47] and regulate the intracellular distribution of APP [21,30]. We hypothesize that X11 and X11L similarly influence the trafficking and/or intracellular localization of HCN1. We further hypothesize that the mislocalization of HCN1 observed in $X11^{-/-}$/$X11L^{-/-}$ mice (Additional file 1: Figure S4) may cause aberrant excitatory neuronal activities, resulting in epileptic seizures.

In conclusion, this study indicates that HCN1 may play an important role in the regulation of neuronal